Theoretical and Computational Aspects of the Optimized Effective Potential Approach Within Density Functional Theory

by

Tim Heaton-Burgess

Department of Chemistry
Duke University

Date: _____

Approved:

_____
Weitao Yang, Advisor

_____
Harold Baranger

_____
David Beratan

_____
Richard MacPhail

Dissertation submitted in partial fulfillment of the requirements for the degree of
Doctor of Philosophy in the Department of Chemistry
in the Graduate School of Duke University
2009

Abstract

(Chemistry – Theoretical and Computational)

Theoretical and Computational Aspects of the Optimized Effective Potential Approach Within Density Functional Theory

by

Tim Heaton-Burgess

Department of Chemistry
Duke University

Date: _____

Approved:

_____
Weitao Yang, Advisor

_____
Harold Baranger

_____
David Beratan

_____
Richard MacPhail

An abstract of a dissertation submitted in partial fulfillment of the requirements for the degree of Doctor of Philosophy in the Department of Chemistry in the Graduate School of Duke University
2009

Abstract

The computational success of density functional theory relies on the construction of suitable approximations to the exchange-correlation energy functional. Use of functional approximations depending explicitly upon the density alone appear unable to address all aspects of many-body interactions, such as the fundamental constraint that the ground state energy is a piecewise linear function of the total number of electrons, and the ability to model nonlocal effects. Functionals depending explicitly upon occupied and unoccupied Kohn–Sham orbitals are considered necessary to address these and other issues. This dissertation considers certain issues relevant to the successful implementation of explicitly orbital-dependent functionals through the optimized effective potential (OEP) approach, as well as extending the potential functional formalism that provides the formal basis for the OEP approach to systems in the presence of noncollinear magnetic fields.

The self-consistent implementation of orbital-dependent energy functionals is correctly done through the optimized effective potential approach – minimization of the ground state energy with respect to the Kohn–Sham potential that generates the set of orbitals employed in the energy evaluation. The focus on the potential can be problematic in finite basis set approaches as determining the exchange-correlation potential in this manner is an inverse problem which, depending upon the combination of orbital and potential basis sets employed, is often ill-posed. The ill-posed nature manifests itself as nonphysical exchange-correlation potentials and total energies.

We address the problem of determining meaningful exchange-correlation potentials for arbitrary combinations of orbital and potential basis sets through an L-curve regularization approach based on biasing towards smooth potentials in the energy minimization. This approach generates physically reasonable potentials for any combination of basis sets as shown by comparisons with grid-based OEP calculations on atoms, and through direct comparison with DFT calculations employing functionals not depending on orbitals for which OEP can also be performed. This work ensures that the OEP methodology can be considered a viable many-body computational methodology.

A separate issue of our OEP implementation is that it can suffer from a lack of size-extensivity – the total energy of a system of infinitely separated monomers may not scale linearly with the total number of monomers depending upon how we construct the Kohn–Sham potential. Typically, a fixed reference potential is employed to aid in the convergence of a finite basis set expansion of the Kohn–Sham potential. This reference potential can be utilized to ensure other desirable properties of the resulting potential. In particular, it can enforce the correct asymptotic behavior. The Fermi–Amaldi potential is often used for this purpose but suffers from size-nonextensivity owing to the explicit dependence of the potential on the total number of electrons. This error is examined and shown to be rather small and rapidly approaches a limiting linear behavior. A size-extensive reference potential with the correct asymptotic behavior is suggested and examined.

We also consider a formal aspect of the potential-based approach that provides the underlying justification of the OEP methodology. The potential functional formalism of Yang, Ayers, and Wu is extended to include systems in the presence of noncollinear magnetic fields. In doing so, a solution to the nonuniqueness issue associated with mapping between potentials and wave functions in such systems is provided, and a computational implementation of the OEP in noncollinear systems is suggested.

Finally, as an example of an issue for which orbital-dependent functionals seem necessary to obtain a correct description, we consider the ground state structures of C_{4N+2} rings which are believed to exhibit a geometric transition from angle-alternation ($N \leq 2$) to bond-alternation ($N > 2$). So far, no published DFT approach has been able to reproduce this behavior owing to the tendency of common density functional approximations to bias towards delocalized electron densities. Calculations are presented with the rCAM-B3LYP exchange-correlation functional that correctly predict the structural evolution of this system. This is rationalized in terms of the recently proposed delocalization error for which rCAM-B3LYP explicitly attempts to address.

Contents

List of Tables

List of Figures

Acknowledgements

I wish to thank my advisor, Professor Weitao Yang, for his relentless encouragement and freedom provided to explore far beyond what is presented within this thesis, particularly so during the last year. His ingenuity have laid the foundation of the research described within this thesis.

I would also like to thank Professor Paul Ayers for discussions and encouragement related to the noncollinear potential formalism described in chapter 2, and Professor Ernest Davidson for raising the issue size-nonextensivity resulting from the use of the Fermi–Amaldi potential described in chapter 4. The L-curve approach described in chapter 3 was investigated concurrently with Doctor Felipe Bulat – he on the inversion of the potential-density mapping and I on the optimized effective potential. Many discussions are acknowledged.

Financial support from the National Institutes of Health, National Science Foundation, and Duke University have been gratefully appreciated.

1

Introduction

1.1 Density and potential based variational principles

The field-free nonrelativistic molecular Hamiltonian within the Born–Oppenheimer approximation,

$$\hat{H} = \sum_{i=1}^{N} -\frac{1}{2}\nabla_i^2 + \sum_{i<j}^{N} \frac{1}{|\mathbf{r}_i - \mathbf{r}_j|} + \sum_{i=1}^{N}\sum_{\alpha=1}^{M} \frac{Z_\alpha}{|\mathbf{r}_i - \mathbf{R}_\alpha|}, \tag{1.1}$$

is completely determined by specification of the total number of electrons, N, and the external field of the nuclei – the nuclear charges, $\{Z_\alpha\}_{\alpha=1}^{M}$, and molecular geometry, $\{\mathbf{R}_\alpha\}_{\alpha=1}^{M}$. For a given N and external field, hereafter denoted as $\hat{V} = \sum_{i=1}^{N} v(\mathbf{r}_i)$, the properties of such a system are determined after mapping on to the corresponding wavefunction through solution of the Schrödinger equation, $\hat{H}\Psi = E\Psi$. Given a physically reasonable wavefunction, the corresponding external potential is determined up to an additive constant (the corresponding energy eigenvalue) through inversion of the Schrödinger equation at any point where the wavefunction does not vanish through

$$\hat{V} - E = -\frac{(\hat{T} + \hat{V}_{\mathrm{ee}})\Psi}{\Psi}, \tag{1.2}$$

where $\hat{T}$ and $\hat{V}_{\text{ee}}$ are the kinetic energy and electron-electron repulsion operators. From this, the uniqueness of mapping between nondegenerate wavefunctions and external potentials modulo an additive constant is established. Studying mappings from the wavefunction to other quantities opens the door for possible computational approaches that do not require the determination of the many-body wavefunction. This is just what the Hohenberg–Kohn (HK) theorem [1] does for non-degenerate ground states by showing that the density uniquely determines the wavefunction (up to a phase factor) and external potential (up to an additive constant). The density depends upon only three spatial variables in comparison to the $3N$ spatial variables of the wavefunction. Given a wavefunction, the corresponding density is determined through quadrature as

$$\rho(\mathbf{r}) = \langle \Psi | \sum_{i=1}^{N} \delta(\mathbf{r} - \mathbf{r}_i) | \Psi \rangle. \tag{1.3}$$

Inversion of a physically reasonable density to find the corresponding wavefunction follows from the variational principle for the total energy in the HK formulation. This ensures that all properties of a system are functionals of the density and that we can obtain that density and the ground state energy, E_{Nv}, of an N-electron system subject to the external potential, v, from a variational formulation as

$$E_{Nv} = \min_{\rho} \; E_{Nv}^{\text{HK}}[\rho] = \min_{\rho} \; \langle \Psi[\rho] | H_{Nv} | \Psi[\rho] \rangle. \tag{1.4}$$

The HK theorem relies on the one-to-one correspondence between nondegenerate ground-state densities and external potentials, so that in the above minimization all trial densities must be able to be generated by some external potential as the corresponding ground state density. This condition is known as v-representability (VR). The condition for a density to be v-representability is not known, and reasonable densities can be explicitly shown to not be v-representable.

The v-representability problem is a significant formal issue but avoidable. The

Levy–Lieb constrained search formalism reformulates the energy functional as [2]

$$E_{Nv} = \min_{\rho} \; E_{Nv}^{\mathrm{LL}}[\rho] = \min_{\rho} \min_{\Psi \to \rho} \langle \Psi | H_{Nv} | \Psi \rangle, \tag{1.5}$$

where the inner minimization searches over all wavefunctions that generate a given density. The condition that a density corresponds to some ground state N-electron wavefunction is known as N-representability. N-representability is satisfied by any nonnegative, integrable, and continuous function [3, 4]. The Levy–Lieb functional also removes the restriction present in the HK functional that the ground state be nondegenerate.

A more recent approach to circumventing the v-representability issue was provided by Yang, Ayers, and Wu [5], which shifted the focus from minimizing with respect to the density onto the external potential, thereby avoiding the issue completely. The ground state energy in this approach is given by

$$E_{Nv} = \min_{w} \; E_{Nv}^{\mathrm{YAW}}[w] = \min_{w} \; \langle \Psi_w | H_{Nv} | \Psi_w \rangle, \tag{1.6}$$

where Ψ_w is the N-electron wavefunction generated by the external potential w through the N-electron Schrödinger equation. This functional is extended to systems in the presence of noncollinear magnetic fields in chapter 2.

1.2 Kohn–Sham DFT

The idea of Kohn and Sham (KS) [6] was to assume the existence of the noninteracting system ($\hat{V}_{\mathrm{ee}} = 0$) that generates the same density as a given interacting system (the noninteracting v-representability assumption). The corresponding KS wavefunction is a single Slater determinant of a set of N orbitals $\{\phi_i\}_{i=1}^{N}$, for which the noninteracting kinetic energy, denoted as T_s, is expressed explicitly in terms of the orbitals as $T_s = -1/2 \sum_{i=1}^{N} \langle \phi_i | \nabla^2 | \phi_i \rangle$, and which recovers a large majority of the physical (interacting) kinetic energy. The remaining kinetic energy component

of the total energy, $T - T_s$, along with the electron-electron interaction minus the classical coulomb energy, $V_{ee} - J$, are lumped together as the exchange-correlation energy $E_{\rm xc}$ as

$$E[\rho] = T[\rho] + V_{\rm ee}[\rho] + \int {\rm d}\mathbf{r}\ v(\mathbf{r})\rho(\mathbf{r}), \tag{1.7}$$

$$= T_s[\rho] + J[\rho] + \int {\rm d}\mathbf{r}\ v(\mathbf{r})\rho(\mathbf{r}) + (T[\rho] + V_{\rm ee}[\rho] - T_s[\rho] - J[\rho]), \tag{1.8}$$

$$= T_s[\rho] + J[\rho] + \int {\rm d}\mathbf{r}\ v(\mathbf{r})\rho(\mathbf{r}) + E_{\rm xc}[\rho]. \tag{1.9}$$

Variation of the energy over continuous square-integrable orbitals under the constraint of orbital orthonormality yields the KS equation,

$$\left(-\frac{1}{2}\nabla^2 + v(\mathbf{r}) + v_J(\mathbf{r}) + v_{xc}(\mathbf{r})\right)\phi_i(\mathbf{r}) = \epsilon_i\phi_i(\mathbf{r}), \tag{1.10}$$

where the potentials are the density-derivatives of the corresponding energy terms and the density is simply

$$\rho(\mathbf{r}) = \sum_{i=1}^{N}\ |\phi_i(\mathbf{r})|^2. \tag{1.11}$$

Equations 1.9, 1.10, and 1.11 are the fundamental relationships required to solve the many body problem within DFT.

An alternative approach to Kohn–Sham DFT is orbital-free DFT (OFDFT) [7]. Here, rather than expressing the Kohn–Sham kinetic energy exactly as a sum over orbitals, it is approximated as a functional of the density. With the total energy functional expressed in terms of the density alone it can be minimized directly under the constraint that the density is normalized. The absence of orbitals permits favorable (linear) scaling with system size, but the additional error that has been introduced by approximating T_s (which is of similar magnitude to the total energy) renders the approach of little use in molecular studies. OFDFT finds favor in large scale calculations where KS DFT is computationally impractical.

1.3 Functional approximations

Approximations to the exchange-correlation energy fall in to two classes – explicit and implicit density functional approximations. Explicit functionals depend solely upon the density and can be further classified according to the form in which the density appears in the functional – local density approximations $E_{\rm xc}^{\rm LDA}[\rho]$ [8, 9], which assume the theory of the uniform electron gas can be applied pointwise to systems where the density varies, and generalized gradient approximations $E_{\rm xc}^{\rm GGA}[\rho, \nabla\rho, \ldots]$ [10] which arise most naturally as a gradient expansion about the uniform electron gas theory. Implicit functionals introduce explicit dependence on the Kohn–Sham orbitals and orbital energies, $E_{\rm xc}[\{\phi_i, \epsilon_i\}]$ [11].

Local approximations are able to generate reasonable geometries, but greatly overbind molecules (by typically 30 kcal/mol for small molecules), overestimate polarizabilities (50%), and underestimate reaction barriers (10 kcal/mol). Gradient approximations significantly improve binding energies but provide much smaller improvement with other properties. Implicit functionals are seen as necessary to approach chemical accuracy ($\sim$ 1 kcal/mol) for thermochemistry, and model nonlocal correlations and the discontinuous nature of the energy under fractional numbers of electrons and fractional spins, although how implicit functionals will be constructed to achieve these requirements is very much an open question.

The simplest example of an implicit density functional is that of Hartree–Fock (exact) exchange,

$$E^{\rm EXX}[\rho] = -\frac{1}{2}\sum_{ij}^{\rm occ} \int {\rm d}\mathbf{r} \int {\rm d}\mathbf{r}' \; \frac{\phi_i(\mathbf{r})\phi_j^*(\mathbf{r})\phi_i^*(\mathbf{r}')\phi_j(\mathbf{r}')}{|\mathbf{r}-\mathbf{r}'|}. \tag{1.12}$$

When treated as a density functional, evaluation of the density-derivative to obtain the local exact exchange potential is not as straightforward as with explicit functionals. The simplest application of the chain rule to evaluate an exchange-correlation

potential from an implicit functional,

$$v_{\mathrm{xc}}(\mathbf{r}) = \frac{\delta E_{\mathrm{xc}}[\rho]}{\delta \rho(\mathbf{r})} = \sum_i \int \mathrm{d}\mathbf{r}' \, \frac{\delta E_{\mathrm{xc}}[\{\phi_i\}]}{\delta \phi_i(\mathbf{r}')} \frac{\delta \phi_i(\mathbf{r}')}{\delta \rho(\mathbf{r})} + \mathrm{c.c.}, \tag{1.13}$$

shows an inverse dependence of orbital variations as a result of density perturbations is introduced, forecasting the possibility of ill-posed aspects of inverse problems appearing in any attempt to construct v_{xc}, which is the topic of chapter 4. The approach to solving for local exchange-correlation potential corresponding to an orbital-dependant exchange-correlation functional is called the optimized effective potential (OEP) approach, as determining the exchange potential with equation 1.13 is equivalent to minimizing the total energy as a functional of the Kohn–Sham potential, as was first noted when observing that solving $\delta E/\delta v_s(\mathbf{r}) = 0$ yields the same equation for v_{xc} as equation 1.13. Such considerations were first introduced in 1953 by Sharp and Horton [12], and first implemented by Talman and Shadwick in 1976 [13]. Details on solving the OEP problem are noted in chapter 4.

The most popular class of implicit density functionals ("hybrid functionals") are formed as a linear combination of the exact exchange energy with explicit density functionals for exchange and correlation. Typical implementations do not calculate the local exchange potential as in equation 1.13, but rather, for each orbital, use the potential obtained from taking the orbital derivative of the exchange energy. This functional derivatives with respect to orbitals (FDO) approach results in a generalized scheme with a nonlocal approximation to the local Kohn–Sham exchange potential

$$\frac{1}{2} \frac{\delta E^{\mathrm{EXX}}[\{\phi_i\}]}{\delta \phi_i^*(\mathbf{r})} = \hat{v}_{\mathrm{x}}^{\mathrm{NL}}(\mathbf{r}) \phi_i(\mathbf{r}). \tag{1.14}$$

For explicit density functionals the two approaches are equivalent. Very little difference is observed between OEP and FDO total energies, although significant improvements have been observed in response properties when treated correctly with

the local OEP [14, 15, 16]. Local approximations to the OEP have also been introduced: the Krieger–Li–Iafrate approximation [17], and the common energy denominator approximation [18]/localized Hartree–Fock [19]/effective local potential [20] approaches. These approximations yield similar total energies to the OEP approach, but poorer response properties.

Hybrid functionals typically improve upon LDA and GGA results in molecular calculations. There are several issues for which all three functional classes yield inadequate results. One notable issue, a manifestation of which will be discussed in chapter 5, is the inability to reproduce the piecewise linear behavior of the total energy as a function of the number of electrons, termed the delocalization error [21]. The delocalization error manifests itself in forms such as overestimation of oligomer polarizabilities [22], incorrect charges on dissociated molecules [23, 24], and underestimation of band gaps [25, 26].

More sophisticated implicit functionals are believed required to target issues such as the delocalization error. Approaches based on perturbation theory using the Kohn–Sham as the reference state [27] and adiabatic connection fluctuation-dissipation [28, 29] correlation energy expressions have shown certain improvement over hybrid functionals. Both of these forms introduce unoccupied (virtual) Kohn–Sham orbitals in to the energy expression, which necessitates an OEP approach for self consistent implementation. The unoccupied orbitals do not contribute to the density but are completely determined by the Kohn–Sham potential. It is unclear what path is the best to take for developing improved functionals, however, the recent work pinpointing fundamental constraints [21] upon the energy provide much needed direction for those seeking to improve density functional approximations to the exchange-correlation energy.

2

Spin-Potential Functional Formalism for Current Carrying Noncollinear Magnetic Systems[1]

2.1 Introduction

In this chapter we develop a formalism dual to spin current density functional theory (CDFT) where minimization with respect to the scalar and vector spin-potentials is utilized. In this way we circumvent the issues surrounding the nonuniqueness of the mapping between spin-potentials and ground-state wavefunctions, and the v-representability issue of current density functionals. The approach applied within the Kohn–Sham formalism provides the foundations for the optimized effective potential (OEP) method for CDFT.

2.2 Background

Spin density functional theory (SDFT) [30, 31, 32, 33] provides the most attractive and computationally accessible *ab-initio* approach for studying the exotic materials typically displaying noncollinear magnetism. Indeed, the application of fully non-

[1] This chapter is based on a previously published paper – Tim Heaton-Burgess, Paul Ayers, and Weitao Yang, Phys. Rev. Lett. 98, 036403 (2007)

collinear SDFT methods is increasing in popularity for both molecular [34, 35] and extended systems [36, 37, 38]. This is despite several undesirable manifestations of the nontrivial degree of nonuniqueness in the mapping between ground-state wavefunctions and external spin-potentials that is peculiar to SDFT. Not much concern had been shown for this issue until recently with renewed discussion on the extent of nonuniqueness and of its implications for practical calculations [39, 40, 41, 42, 43], the most significant being the discontinuous nature of the exchange-correlation energy as a functional of the electron density [39, 41]. The development presented here incorporates directly the nonuniqueness with well defined functionals, whilst providing a method for the optimized effective potential approach beyond the conventional local and semi-local approximations typically used in SDFT. Our formulation, based upon minimization with respect to scalar and vector spin-potentials, provides the formal justification that is lacking from existing approaches to the CDFT OEP. Further, it lends itself to novel implementations where the minimization property can be exploited, rather than solving coupled integral equations as is done in more conventional approaches.

For nondegenerate ground-states of systems in the absence of noncollinear magnetic fields, the Hohenberg-Kohn (HK) theorem [1] ensures the existence of the bijective (invertible) mapping between scalar external potentials (modulo an additive constant) and their corresponding ground-state density. This, together with the Kohn–Sham implementation [6], has allowed the development of density-functional theory as an extremely successful approach to the many-body problem [44].

Extensions to incorporate ground state spin densities followed straightforwardly, but also introduces a subtle issue of nonuniqueness in the mapping between external spin-potentials and ground-state wavefunctions. In this situation there are two independent spin potentials v_α and v_β, and specifying the zero of energy can only uniquely determine one potential, leaving the other undeterminable up to some ad-

ditive constant [39]. The inclusion of noncollinear fields can lead to less trivial forms of nonuniqueness. This was first observed in the seminal work of von Barth and Hedin [30], who exemplified such nonuniqueness in one-electron systems by explicit construction. The question of whether such behavior is present in many-electron systems was only recently addressed [39, 40, 41] with the systematic characterization of the potentials yielding the same ground-state density in both current free and current carrying systems. For a current-free system, this is achieved by considering the scalar potential and magnetic field, $v'(\mathbf{r}) = v(\mathbf{r}) + \Delta v(\mathbf{r})$ and $\mathbf{B}'(\mathbf{r}) = \mathbf{B}(\mathbf{r}) + \Delta\mathbf{B}(\mathbf{r})$, where $v'(\mathbf{r})$ and $\mathbf{B}'(\mathbf{r})$ are presumed to have the same ground state as $v(\mathbf{r})$ and $\mathbf{B}(\mathbf{r})$. The condition for this to occur is that

$$\int \mathrm{d}\mathbf{r} \;\left(\hat{\rho}(\mathbf{r})\Delta v(\mathbf{r}) - \hat{\mathbf{m}}(\mathbf{r})\Delta\mathbf{B}(\mathbf{r})\right)\Psi = \Delta E\Psi, \tag{2.1}$$

where $\hat{\mathbf{m}}(\mathbf{r})$ is the magnetization operator and ΔE is the difference in ground state energies of Ψ in the primed and unprimed fields. A solution for $\Delta v(\mathbf{r})$ and $\Delta\mathbf{B}(\mathbf{r})$ is said to give rise to systematic nonuniqueness if it corresponds to a linear combination of $\hat{\rho}(\mathbf{r})$ and $\hat{\mathbf{m}}(\mathbf{r})$ that is a constant of motion of the system, and accidental nonuniqueness otherwise.

Here we develop, irrespective of the extent of nonuniqueness occuring in a given system, a transparent formalism for current-carrying noncollinear magnetic systems by using the spin-potentials as the fundamental variables. This approach was recently developed for field-free systems [5] as a rigorous foundation for the optimized effective potential approach. This work also provided a solution to the v-representability (VR) issue in the HK formulation of DFT without extending the domain of the functionals to non-VR densities (as is done, for example, in the constrained search approach [2]). The VR issue is also present within SDFT in terms of $v_{\sigma\sigma'}$-representability (or $(v_{\sigma\sigma'},\mathbf{A}_\sigma)$-representability for spin-current density functional theory).

2.3 Formalism

Let us consider a nonrelativistic N-electron system in the presence of a scalar external potential $v(\mathbf{r})$ and noncollinear magnetic field $\mathbf{B}(\mathbf{r})$ with the Hamiltonian [45]

$$\hat{H}_{v_{\sigma\sigma'},\mathbf{A}_\sigma} = \hat{T} + \hat{V}_{\mathrm{ee}} + \hat{V}_{v_{\sigma\sigma'},\mathbf{A}_\sigma}. \tag{2.2}$$

Here the external potential characterized by a given set of spin-potentials $(v_{\sigma\sigma'}, \mathbf{A}_\sigma)$ has been expressed as

$$\hat{V}_{v_{\sigma\sigma'},\mathbf{A}_\sigma} = \int \mathrm{d}\mathbf{r} \left(\sum_\sigma \hat{\mathbf{j}}_{p,\sigma}(\mathbf{r}) \cdot \mathbf{A}_\sigma(\mathbf{r}) + \sum_{\sigma\sigma'} \hat{\rho}_{\sigma\sigma'}(\mathbf{r}) \left(v_{\sigma\sigma'}(\mathbf{r}) + \frac{1}{2}\delta_{\sigma\sigma'}\mathbf{A}_\sigma^2(\mathbf{r}) \right) \right), \tag{2.3}$$

where $v_{\sigma\sigma'}(\mathbf{r}) = v(\mathbf{r})\delta_{\sigma\sigma'} - \mu_{\mathrm{B}}\mathbf{B}(\mathbf{r}) \cdot \boldsymbol{\sigma}_{\sigma\sigma'}$, $\boldsymbol{\sigma}_{\sigma\sigma'}$ is the vector of Pauli spin matrix components and the magnetic field and vector potential are related by $\mathbf{B}(\mathbf{r}) = \nabla \times \mathbf{A}(\mathbf{r})$. The spin resolved density and paramagnetic current density operators are given by $\hat{\rho}_{\sigma\sigma'}(\mathbf{r}) = \sum_{j=1}^N |\sigma'(s_j)\rangle\delta(\mathbf{r} - \mathbf{r}_j)\langle\sigma(s_j)|$ and $\hat{\mathbf{j}}_{p,\sigma}(\mathbf{r}) = -\frac{i}{2}\sum_{j=1}^N |\sigma(s_j)\rangle(\nabla_j\delta(\mathbf{r} - \mathbf{r}_j) + \delta(\mathbf{r} - \mathbf{r}_j)\nabla_j)\langle\sigma(s_j)|$ respectively, where our notation $|\sigma'(s_j)\rangle\langle\sigma(s_j)|$ couples the σ and σ' components of the j'th electron.

The fundamental variables within CDFT are usually taken as the N-representable density ρ, magnetization $\mathbf{m}(\mathbf{r})$, and paramagnetic current-density $\mathbf{j}_p$. A variational energy functional of the density variables which bypasses the v-representability constraint is then constructed using the constrained search formalism as [46] $E[\rho, \mathbf{m}, \mathbf{j}_p] = \min_{\Psi\to(\rho,\mathbf{m},\mathbf{j}_p)}\langle\Psi|\hat{T} + \hat{W} + \hat{V}|\Psi\rangle$. Minimizing $E[\rho, \mathbf{m}, \mathbf{j}_p]$ under the constraint of N-representability yields the ground-state energy. We wish to depart from this conventional viewpoint of current density functionals to focus, instead, on the spin-potentials dual to the spin-densities as fundamental variables. In this way, let us denote the wavefunction corresponding to a given set of potentials $(w_{\sigma\sigma'}, \mathbf{a}_\sigma)$ as $\Psi_{w_{\sigma\sigma'},\mathbf{a}_\sigma}$ and define a energy spin-potential functional as

$$E^1_{N,v_{\sigma\sigma'},\mathbf{A}_\sigma}[w_{\sigma\sigma'}, \mathbf{a}_\sigma] = \langle\Psi_{w_{\sigma\sigma'},\mathbf{a}_\sigma}|\hat{H}_{v_{\sigma\sigma'},\mathbf{A}_\sigma}|\Psi_{w_{\sigma\sigma'},\mathbf{a}_\sigma}\rangle. \tag{2.4}$$

The superscript 1 indicates full interaction between electrons. This definition assumes at least one bound state (with the convention that a bound state has negative energy) exists for a given set of potentials. If this is not the case, the functional is generalized to $E^1_{N,v_{\sigma\sigma'},\mathbf{A}_\sigma}[w_{\sigma\sigma'},\mathbf{a}_\sigma] = \min_{0<M<N} E^1_{M,v_{\sigma\sigma'},\mathbf{A}_\sigma}[w_{\sigma\sigma'},\mathbf{a}_\sigma]$, where the minimization over $0 < M < N$ includes only those states where all electrons are bound. If no such state exists, then $E^1_{N,v_{\sigma\sigma'},\mathbf{A}_\sigma}[w_{\sigma\sigma'},\mathbf{a}_\sigma] = 0$.

We immediately observe that the Rayleigh–Ritz variational principle provides the ground-state energy as a lower bound to our functional:

$$\begin{aligned} E_{N,v_{\sigma\sigma'},\mathbf{A}_\sigma} &= E^1_{N,v_{\sigma\sigma'},\mathbf{A}_\sigma}[v_{\sigma\sigma'},\mathbf{A}_\sigma], \\ &= \min_{w_{\sigma\sigma'},\mathbf{a}_\sigma} E^1_{N,v_{\sigma\sigma'},\mathbf{A}_\sigma}[w_{\sigma\sigma'},\mathbf{a}_\sigma]. \end{aligned} \tag{2.5}$$

There may be many minimizing potentials in addition to the true external potentials of our system [30, 40, 39, 41]. However, that is of little consequence and indeed extends the set of meaningful potentials, for any such minimizing potential can be used to extract the ground state energy. The stationary nature of $E^1_{N,v_{\sigma\sigma'},\mathbf{A}_\sigma}[w_{\sigma\sigma'},\mathbf{a}_\sigma]$ is most readily examined by rewriting the functional in the form

$$\begin{aligned} E^1_{N,v_{\sigma\sigma'},\mathbf{A}_\sigma}[w_{\sigma\sigma'},\mathbf{a}_\sigma] &= E^1_{N,w_{\sigma\sigma'},\mathbf{a}_\sigma}[w_{\sigma\sigma'},\mathbf{a}_\sigma] \\ &+ \sum_\tau \int \mathrm{d}\mathbf{r}\ \mathbf{j}_{p\tau;w_{\sigma\sigma'},\mathbf{a}_\sigma}(\mathbf{r}) \cdot (\mathbf{A}_\tau(\mathbf{r}) - \mathbf{a}_\tau(\mathbf{r})) \\ &+ \frac{1}{2}\sum_\tau \int \mathrm{d}\mathbf{r}\ \rho_{\tau\tau;w_{\sigma\sigma},\mathbf{a}_\sigma}(\mathbf{r})(\mathbf{A}^2_\tau(\mathbf{r}) - \mathbf{a}^2_\tau(\mathbf{r})) \\ &+ \sum_{\tau\tau'} \int \mathrm{d}\mathbf{r}\ \rho_{\tau\tau';w_{\sigma\sigma'},\mathbf{a}_\sigma}(\mathbf{r})(v_{\tau\tau'}(\mathbf{r}) - w_{\tau\tau'}(\mathbf{r})), \end{aligned} \tag{2.6}$$

where $E^1_{N,w_{\sigma\sigma'},\mathbf{a}_\sigma}[w_{\sigma\sigma'},\mathbf{a}_\sigma]$ is the ground state energy of a system with external potentials $w_{\sigma\sigma'}(\mathbf{r})$ and $\mathbf{a}_\sigma(\mathbf{r})$, and has the functional derivatives $\delta E^1_{N,w_{\sigma\sigma'},\mathbf{a}_\sigma}[w_{\sigma\sigma'},\mathbf{a}_\sigma]/\delta w_{\tau\tau'} = \rho_{\tau\tau';w_{\sigma\sigma'},\mathbf{a}_\sigma}$ and $\delta E^1_{N,w_{\sigma\sigma'},\mathbf{a}_\sigma}[w_{\sigma\sigma'},\mathbf{a}_\sigma]/\delta \mathbf{a}_\tau = \mathbf{j}_{p\tau;w_{\sigma\sigma'},\mathbf{a}_\sigma} + \rho_{\tau\tau;w_{\sigma\sigma'},\mathbf{a}_\sigma}\mathbf{a}_\tau$. Utilizing these,

we obtain

$$\frac{\delta E^1_{N,v_{\sigma\sigma'},\mathbf{A}_\sigma}[w_{\sigma\sigma'},\mathbf{a}_\sigma]}{\delta w_{\tau\tau'}(\mathbf{r})} =$$

$$\sum_{\mu\mu'}\int \mathrm{d}\mathbf{r}'\,\left(\frac{\delta\rho_{\mu\mu';w_{\sigma\sigma'},\mathbf{a}_\sigma}(\mathbf{r}')}{\delta w_{\tau\tau'}(\mathbf{r})}\left(v_{\mu\mu'}(\mathbf{r}')-w_{\mu\mu'}(\mathbf{r}')+\frac{1}{2}\delta_{\mu\mu'}\big(\mathbf{A}^2_\mu(\mathbf{r}')-\mathbf{a}^2_\mu(\mathbf{r}')\big)\right)\right)$$

$$+\sum_\mu\int \mathrm{d}\mathbf{r}'\,\frac{\delta\mathbf{j}_{p\mu;w_{\sigma\sigma'},\mathbf{a}}(\mathbf{r}')}{\delta w_{\tau\tau'}(\mathbf{r})}\cdot\Big(\mathbf{A}_\mu(\mathbf{r}')-\mathbf{a}_\mu(\mathbf{r}')\Big), \tag{2.7}$$

and

$$\frac{\delta E^1_{N,v_{\sigma\sigma'},\mathbf{A}_\sigma}[w_{\sigma\sigma'},\mathbf{a}_\sigma]}{\delta \mathbf{a}_{\tau}(\mathbf{r})} =$$

$$\sum_{\mu\mu'}\int \mathrm{d}\mathbf{r}'\,\left(\frac{\delta\rho_{\mu\mu';w_{\sigma\sigma'},\mathbf{a}_\sigma}(\mathbf{r}')}{\delta \mathbf{a}_{\tau}(\mathbf{r})}\left(v_{\mu\mu'}(\mathbf{r}')-w_{\mu\mu'}(\mathbf{r}')+\frac{1}{2}\delta_{\mu\mu'}\big(\mathbf{A}^2_\mu(\mathbf{r}')-\mathbf{a}^2_\mu(\mathbf{r}')\big)\right)\right)$$

$$+\sum_\mu\int \mathrm{d}\mathbf{r}'\,\frac{\delta\mathbf{j}_{p\mu;w_{\sigma\sigma'},\mathbf{a}_\sigma}(\mathbf{r}')}{\delta \mathbf{a}_{\tau}(\mathbf{r})}\Big(\mathbf{A}_\mu(\mathbf{r}')-\mathbf{a}_\mu(\mathbf{r}')\Big). \tag{2.8}$$

A solution to the stationary conditions is clearly seen to be $w_{\sigma\sigma'}(\mathbf{r}) = v_{\sigma\sigma'}(\mathbf{r})$ and $\mathbf{a}_\sigma(\mathbf{r}) = \mathbf{A}_\sigma(\mathbf{r})$. The response functions appearing in these equations may have nontrivial null spaces because of the nonunique mapping between spin-potentials and spin-densities. If this is the case we will have further stationary points $w_{\sigma\sigma'}(\mathbf{r}) = v_{\sigma\sigma'}(\mathbf{r}) + g_{\sigma\sigma'}(\mathbf{r})$ and $\mathbf{a}_\sigma(\mathbf{r}) = \mathbf{A}_\sigma(\mathbf{r}) + \mathbf{h}_\sigma(\mathbf{r})$, where $g_{\sigma\sigma'}$ and $\mathbf{h}_\sigma$ are elements of the appropriate null spaces. In particular, these additional solutions include all those situations for which the spin-potential-wavefunction mapping is nonunique. We have thus shown that the global minima corresponding to both the true external spin-potentials and any arising due to nonuniqueness are stationary points in the potential space.

To construct a practical realization of this work we develop a Kohn–Sham approach. Consider a noninteracting KS system with spin-density $\rho_{\sigma\sigma';w_{s,\sigma\sigma'}\mathbf{a}_{s,\sigma}}(\mathbf{r})$ and

spin-current density $\mathbf{j}_{p\sigma;w_{s,\sigma\sigma'}\mathbf{a}_{s,\sigma}}(\mathbf{r})$, expressed in terms of the spinor orbital components of the KS equation

$$\frac{1}{2}\big(-i\nabla+\mathbf{a}_{s,\sigma}(\mathbf{r})\big)^2\psi_{i\sigma;w_{s,\sigma\sigma'}\mathbf{a}_\sigma}(\mathbf{r}) + \sum_{\sigma'} w_{s,\sigma\sigma'}(\mathbf{r})\psi_{i\sigma';w_{s,\sigma\sigma'}\mathbf{a}_\sigma}(\mathbf{r}) = \epsilon_{i;w_{s,\sigma\sigma'}\mathbf{a}_\sigma}\psi_{i\sigma;w_{s,\sigma\sigma'}\mathbf{a}_\sigma}(\mathbf{r}). \tag{2.9}$$

As is usual in DFT, we must make the assumption of Kohn–Sham v-representability (KSVR) – the existence of at least one set of potentials such that $\rho_{\sigma\sigma';w_{s,\sigma\sigma'}\mathbf{a}_{s,\sigma}} = \rho_{\sigma\sigma';w_{\sigma\sigma'}\mathbf{a}_\sigma}$ and $\mathbf{j}_{p\sigma;w_{s,\sigma\sigma'}\mathbf{a}_{s,\sigma}} = \mathbf{j}_{p\sigma;w_{\sigma\sigma'}\mathbf{a}_\sigma}$. The nonuniqueness arises once again with the possibility of many KS spin-potentials existing that yield the spin-densities of interest. But such nonuniqueness is not an issue here because it merely represents degenerate solutions to the minimization of the ground-state potential functional. To describe the ground state, all we need is to find one of the degenerate solutions.

Define an energy spin-potential functional for the KS system as

$$\begin{aligned} &E^0_{N,v_{\sigma\sigma'},\mathbf{A}_\sigma}[w_{s,\sigma\sigma'},\mathbf{a}_{s,\sigma}] = \\ &T_s[\rho_{\sigma\sigma';w_{s,\sigma\sigma'},\mathbf{a}_{s,\sigma}},\mathbf{j}_{p\sigma;w_{s,\sigma\sigma'},\mathbf{a}_{s,\sigma}}] + J[\rho_{\sigma\sigma';w_{s,\sigma\sigma'},\mathbf{a}_{s,\sigma}}] + E_{\rm xc}[\rho_{\sigma\sigma';w_{s,\sigma\sigma'},\mathbf{a}_{s,\sigma}},\mathbf{j}_{p\sigma;w_{s,\sigma\sigma'},\mathbf{a}_{s,\sigma}}] \\ &+\sum_{\tau\tau'}\int \mathrm{d}\mathbf{r}\ \left(v_{\tau\tau'}(\mathbf{r})+\frac{1}{2}\delta_{\tau\tau'}\mathbf{A}^2_\tau(\mathbf{r})\right)\rho_{\tau\tau';w_{s,\sigma\sigma'},\mathbf{a}_s}(\mathbf{r}) + \sum_\tau\int \mathrm{d}\mathbf{r}\ \mathbf{j}_{p\tau;w_{s,\sigma\sigma'},\mathbf{a}_{s,\sigma}}(\mathbf{r})\cdot\mathbf{A}_\tau(\mathbf{r}), \end{aligned} \tag{2.10}$$

where the decomposition is in terms of the KS kinetic energy T_s, Coulomb energy J, and exchange-correlation energy $E_{\rm xc}$ functionals. For the KS energy defined as $E^{\rm KS}_{N,v_{\sigma\sigma'},\mathbf{A}_\sigma} = \inf_{w_{s,\sigma\sigma'},\mathbf{a}_{s,\sigma}} E^0_{N,v_{\sigma\sigma'},\mathbf{A}_\sigma}[w_{s,\sigma\sigma'},\mathbf{a}_{s,\sigma}]$, we see that as long as $\rho_{v_{\sigma\sigma'},\mathbf{a}_s}(\mathbf{r})$ is

KSVR, $E^{\rm KS}_{N,v_{\sigma\sigma'},\mathbf{A}_\sigma} = E_{N,v_{\sigma\sigma'},\mathbf{A}_\sigma}$. The functional derivatives of $E^0_{N,v_{\sigma\sigma'},\mathbf{A}}$ are

$$\frac{\delta E^0_{N,v_{\sigma\sigma'},\mathbf{A}_{s,\sigma}}[w_{s,\sigma\sigma'},\mathbf{a}_{s,\sigma}]}{\delta w_{s,\tau\tau'}(\mathbf{r})} =$$

$$\sum_{\mu\mu'}\int \mathrm{d}\mathbf{r}'\,\left(\frac{\delta\rho_{\mu\mu';w_{s,\sigma\sigma'},\mathbf{a}_{s,\sigma}}(\mathbf{r}')}{\delta w_{s,\tau\tau'}(\mathbf{r})}\left(v_{\mathrm{eff},\mu\mu'}(\mathbf{r}')-w_{s,\mu\mu'}(\mathbf{r}')\right)\right.$$

$$\left.+\,\delta_{\mu,\mu'}\frac{\delta\mathbf{j}_{p\mu;w_{s,\sigma\sigma'},\mathbf{a}_{s,\sigma}}(\mathbf{r}')}{\delta w_{s,\tau\tau'}(\mathbf{r})}\cdot\left(\mathbf{A}_{\mathrm{eff},\mu}(\mathbf{r}')-\mathbf{a}_{s,\mu}(\mathbf{r}')\right)\right), \tag{2.11}$$

and

$$\frac{\delta E^0_{N,v_{\sigma\sigma'},\mathbf{A}}[w_{s,\sigma\sigma'},\mathbf{a}_{s,\sigma}]}{\delta \mathbf{a}_{s,\tau}(\mathbf{r})} =$$

$$\sum_{\mu\mu'}\int \mathrm{d}\mathbf{r}'\,\left(\frac{\delta\rho_{\mu\mu';w_{s,\sigma\sigma'},\mathbf{a}_{s,\sigma}}(\mathbf{r}')}{\delta \mathbf{a}_{s,\tau}(\mathbf{r})}\left(v_{\mathrm{eff},\mu\mu'}(\mathbf{r}')-w_{s,\mu\mu'}(\mathbf{r}')\right)\right.$$

$$\left.+\,\delta_{\mu,\mu'}\frac{\delta\mathbf{j}_{p\mu;w_{s,\sigma\sigma'},\mathbf{a}_{s,\sigma}}(\mathbf{r}')}{\delta \mathbf{a}_{s,\sigma}(\mathbf{r})}\left(\mathbf{A}_{\mathrm{eff},\mu}(\mathbf{r}')-\mathbf{a}_{s,\mu}(\mathbf{r}')\right)\right). \tag{2.12}$$

Here we have defined the KS effective spin-potentials $v_{\mathrm{eff},\tau\tau'} = v_{\tau\tau'} + v_{J,\tau\tau'} + v_{\mathrm{xc},\tau\tau'} + \frac{1}{2}\delta_{\tau\tau'}(\mathbf{A}^2_\tau - \mathbf{A}^2_{\mathrm{eff},\tau})$, $\mathbf{A}_{\mathrm{eff},\tau} = \mathbf{A}_\tau + \mathbf{A}_{\mathrm{xc},\tau}$ with $v_{\mathrm{xc},\tau\tau'} = \delta E_{\mathrm{xc}}/\delta\rho_{\tau\tau';w_{s,\sigma\sigma'},\mathbf{a}_{s,\sigma}}$ and $\mathbf{A}_{\mathrm{xc},\tau} = \delta E_{\mathrm{xc}}/\delta\mathbf{j}_{p\tau;w_{s,\sigma\sigma'},\mathbf{a}_{s,\sigma}}$. Note that to stay within KSVR densities, density derivatives of orbital functionals such as the exchange-correlation potentials must be evaluated by invoking the chain rule, so that only orbital derivatives of the functional are required. Imposing the stationary condition, one finds the solutions

$$w_{s,\sigma\sigma'}(\mathbf{r}) = v_{\mathrm{eff},\sigma\sigma'}(\mathbf{r}) + g_{s,\sigma\sigma'}(\mathbf{r}), \tag{2.13}$$

$$\mathbf{a}_s(\mathbf{r}) = \mathbf{A}_{\mathrm{eff},\sigma}(\mathbf{r}) + \mathbf{h}_{s,\sigma}(\mathbf{r}), \tag{2.14}$$

for $g_{s,\sigma\sigma'}$ and $\mathbf{h}_{s,\sigma}$ in the null spaces of the appropriate noninteracting response functions. This result is in agreement with conventional CDFT [47, 45], but goes beyond it in explicitly incorporating any nonuniqueness in the mapping between the noninteracting spin-potentials and the spin-density.

As with the constrained-search approach, this dual formulation of CDFT solves the v-representability issue that would exist in a HK approach. The relationship between the potential functional and density functional approaches is illustrated in Fig. 2.1. An energy density functional $E_{N,v_{\sigma\sigma'},\mathbf{A}_\sigma}[\rho_{\sigma\sigma'},\mathbf{j}_{p\sigma}]$ is defined only on the set of v-representable densities for which the potential-density relation exists. Minimizing $E_{N,v_{\sigma\sigma'},\mathbf{A}_\sigma}[\rho_{\sigma\sigma'},\mathbf{j}_{p\sigma}]$ subject to the constraint that the trial densities must belong to this set then yields the ground-state energy. Our dual approach utilizing the potential functional $E^1_{N,v_{\sigma\sigma'},\mathbf{A}_\sigma}[w_{\sigma\sigma'},\mathbf{a}_\sigma]$ is defined for all physical potentials and yields the ground state energy after an unconstrained minimization. Both approaches must invoke the KSVR assumption to construct a feasible implementation. The noninteracting functional $E^0_{N,v_{\sigma\sigma'},\mathbf{A}_\sigma}[w_{\sigma\sigma'},\mathbf{a}_\sigma]$ yields the KS energy under an unconstrained minimization and thus provides a rigorous foundation for the OEP procedure. For both of our potential functionals, any nonuniqueness in the potential-wavefunction mapping is manifested in the stationary conditions.

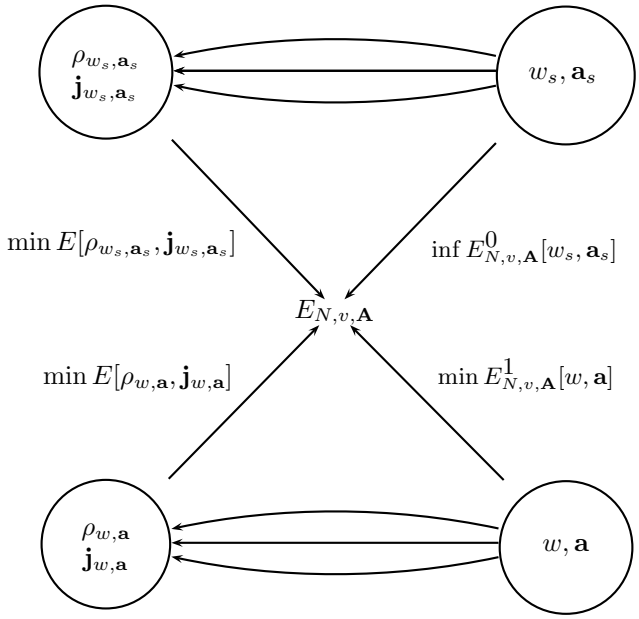

FIGURE 2.1: Potential functional – density functional duality.

2.4 Proposed implementation

In analogy to the direct OEP method of Yang and Wu [48], this formalism motivates a novel OEP implementation that does not require an integral equation to be solved in conventional CDFT OEP implementations. One expands the KS external spin-potentials in a basis set as

$$v_{s\sigma\sigma'}(\mathbf{r}) = v_{\sigma\sigma'}(\mathbf{r}) + v_0(\mathbf{r}) + \sum_j c_j^{\sigma\sigma'} g_j(\mathbf{r}), \tag{2.15}$$

$$\mathbf{A}_{s\sigma}(\mathbf{r}) = \mathbf{A}_{\sigma}(\mathbf{r}) + \mathbf{A}_0(\mathbf{r}) + \sum_j d_j^{\sigma} \mathbf{h}_j(\mathbf{r}), \tag{2.16}$$

where $v_{\sigma\sigma'}(\mathbf{r})$ and $\mathbf{A}_{\sigma}(\mathbf{r})$ are the external potentials of our system of interest consistent with $\mathbf{B} = \nabla \times \mathbf{A}$, $v_0(\mathbf{r})$ and $\mathbf{A}_0(\mathbf{r})$ are fixed reference potentials, and $\{c_j^{\sigma\sigma'}, d_j^{\sigma}\}$ are the coefficients of the potential expansion to be determined. The reference potentials should be chosen to enforce appropriate asymptotic behavior and aid in the basis set convergence. Once an energy functional of the spin-orbitals $E[\{\phi_{i,\sigma}\}]$ is given, the OEP problem is transformed into a minimization problem with respect to the potential expansion coefficients. The derivatives $\partial E(\{c_j^{\sigma\sigma'}, d_j^{\sigma}\})/\partial c_j^{\sigma\sigma'} = \int \mathrm{d}\mathbf{r}\, \delta E/\delta v_{s\sigma\sigma'}(\mathbf{r}) g_j(\mathbf{r})$, and analogously $\partial E(\{c_j^{\sigma\sigma'}, d_j^{\sigma}\})/\partial d_j^{\sigma}$, are available in a simple form allowing the problem to be solved efficiently by conventional iterative optimization, providing an alternative approach to that recently developed by Sharma *et al.* [49] and Rohra and Görling [50]. However, these conventional approaches to the OEP problems are based on the *assumption* that the desired solutions correspond to solving $\delta E/\delta v = 0$ and $\delta E/\delta \mathbf{A} = \mathbf{0}$. Under this assumption, the problem is transformed into two coupled integral equations. Our direct approach rigourously justifies seeking the potential that minimizes E^0, and establishes that this solution is a stationary point in the potential space. Formulating the OEP problem in this way – i.e., as an unconstrained minimization problem with readily available derivatives –

allows one to exploit conventional optimization methods and offers the prospect of an efficient and robust implementation for molecules and extended systems.

2.5 Conclusion

We have shown how the potential-based formalism of Yang, Ayers, and Wu can be extended to systems in the presence of noncollinear fields. In doing so we are able to bypass the issues of v-representability and nonuniqueness when mapping between external potentials and wavefunctions in such systems. The approach provides the formal justification for the OEP methodology, and motivates a direct minimization implementation of the OEP.

3

Optimized Effective Potentials from Arbitrary Basis Sets[1]

3.1 Introduction

We now move on from the formal discussion of potential-based approaches to a practical realization of the potential functional formalism – the optimized effective potential (OEP) method – were we will address an undesirable aspect of its implementation. The issues involved straddle both formal and computational aspects of the OEP, the determination of which is a nonlinear inverse problem. Our work deals only with the field-free situation, but the concepts developed could readily be extended to systems in the presence of noncollinear fields.

Direct physical problems pervade quantum chemistry – we typically have a precise definition of our system, the nuclei and electrons, and under appropriate boundary conditions we attempt to solve in some manner a Schrödinger (or Kohn–Sham) equation to map us on to our solution for a wavefunction (or density). The forward nature of such approaches make them in many senses computationally well-posed, regardless

[1] This chapter is based on a previously published paper – Tim Heaton-Burgess and Weitao Yang, J. Chem. Phys. 129, 194102 (2008)

of the precise physical nature of the system of interest.

Whilst less prevalent, inverse problems also appear in many areas of theoretical chemistry. We can broadly distinguish two philosophies based on whether we wish to rigorously reconstruct a physically meaningful property or, if in an attempt to gain some chemical insight, we try to construct using a certain amount of chemical intuition an appealing (albeit arbitrarily defined) quantity from a more general global property. Two examples of the latter are the multitude of atom-in-molecule approaches where one partitions a molecular density into localized atomic densities (examples being [51, 52, 53, 54]), and the related construction of atom condensed Fukui functions [55, 56] from the completely rigorous global Fukui function [57].

Rigorously defined inverse problems seek the physical cause of an observed property. Very often we are seeking a potential that generates, for example, a given wavefunction, density [58, 59, 60, 61, 62], or some physically desirable property [63, 64]. Irrespective of what we are reconstructing, such tasks are inevitably much more difficult to solve in a satisfying manner owing to the ill-posed nature that is common to most all inverse problem [65, 66]: A poorly thought out approach to solving inverse problems has the likelihood of nonphysical ramifications owing to a lack of stability in forming these inverse mappings. Computationally this is manifested as an extreme sensitivity towards our input data and nonuniqueness of the reconstructed property. This however does not imply, in general, that the original problem has been incorrectly formulated.

As with most electronic structure methodologies, the conventional approach (using explicit density functionals) to DFT is a direct problem – given an approximate exchange-correlation functional, the corresponding exchange-correlation potential determines the density and subsequently the energy.

In the effort to construct better functionals there is significant interest to incorporate an implicit dependance upon the density by explicitly including some

functional dependance upon KS orbitals and orbital energies within the exchange-correlation functional. For such implicit functionals we cannot simply construct the local derivative $\delta E_{\rm xc}[\{\phi_i\}]/\delta\rho$ to yield the corresponding exchange-correlation potential. Rather we must construct that $v_{\rm xc}$ which generates the set of KS orbitals that minimizes the total energy functional – an inverse problem that is the OEP approach for implicit density functionals which has been of considerable interest recently [67, 20, 68, 69, 70, 71, 72].

The efficient implementation of the OEP method for molecular systems is commonly accomplished by employing finite basis approaches for the exchange-correlation potential [73, 74, 48, 75] which in turn gives rise to the computational issues of an ill-posed inverse problem. Any finite basis set construction of the exchange-correlation potential is limited to some degree in what it can represent. Further, in this inverse setting it is also limited in regards to orbital perturbations in which it can react to. As such the basis set for the potential, and that for the orbitals, can possibly be inappropriate in that changes in the potential basis set could not be manifested in the orbitals if, say, a disturbance in the potential is created in a region where the orbitals will vanish due to the basis set form, or if the potential changes in such a rapid, nonphysical manner, that the orbitals cannot adjust. This lays at the heart of the issues seen with OEP problems – the possibility to generate many (infinite) overtly nonphysical potentials, all giving rise to a common set of orbitals which in a finite basis representation solve the KS equations.

The occurrence of nonphysical oscillations in exact-exchange OEP's has been noted for some time [76]. More recently the issues at hand have been made dramatically clear by Staroverov *et al.* [67] who, for any orbital basis set, showed how to construct infinitely many local exact-exchange potentials (with varying degrees of nonphysicality) that yield identically the Hartree-Fock energy by constructing finite-basis exchange potentials in a manner such that $\delta E^{\rm HF}[\{\phi_i^{\rm KS}\}]/\delta\phi_i^{\rm KS} = 0$ – the

Hartree-Fock stationarity condition for orbitals derived from a local potential. In the complete basis set limit OEP and HF energies are expected, in general, to differ [77]. This coincidence of finite basis ground-state OEP and HF energies raised questions of the usefulness of the OEP method and spurred significant effort to develop computationally robust approaches for solving the OEP problem. The fundamental question raised by the work of Staroverov *et al.*, which we have previously addressed [78] and will further investigate in the current chapter, is: *Given an arbitrary orbital basis set, and an arbitrary potential basis set, how can we construct a meaningful optimized effective potential?* Heßelmann *et al.* [69] have recently considered a related but different question: Given a potential basis set, how does one construct an orbital basis set that yields a numerically stable optimized effective potential. The resulting orbital basis sets are extremely large, making it difficult for practical applications in chemistry. In addition, in doing so the established prescription of the orbital basis set being part of the defining model for electronic structure calculations is lost. If the OEP is to become a routinely used quantum chemical method, the necessity for reciprocation with the more established approaches demands that the selection of orbital basis not be demoted in this manner and be prescribed as part of the calculation model.

This chapter is organized as follows: Sections 3.2 and 3.3 review the formal and computational setting of the Yang–Wu OEP method. In Sec. 3.4 we discuss our new regularization method for performing OEP calculations with arbitrary basis sets and provide analysis on the possible structure of the OEP L-curve and the choice of the optimal potential and energy. Section 5 presents results related to the energies our approach obtains, provides comparisons with other finite basis OEP methods, and investigates the best way to select the optimal potential from the L-curve.

3.2 Theoretical Background

The optimized effective potential approach determines the local external potential (the Kohn–Sham potential) of a noninteracting system that minimizes the ground state energy of a given interacting system characterized by an external potential v. Denoting the functional dependance of a ground state N-electron determinental wavefunction upon a trial potential as Φ_{w_s}, we rigorously state the OEP problem as [5]

$$E_{N,v}^{\mathrm{OEP}} = \min_{w_s(\mathbf{r})} \langle \Phi_{w_s} | \hat{H}_v | \Phi_{w_s} \rangle, \tag{3.1}$$

where the potential w_s determines a corresponding set of orbitals and eigenvalues as

$$\left(-\frac{1}{2}\nabla^2 + w_s(\mathbf{r}) \right) \phi_{w_s,i}(\mathbf{r}) = \epsilon_{w_s,i} \phi_{w_s,i}(\mathbf{r}). \tag{3.2}$$

The original approach to solving for the OEP is based on expressing the exchange-correlation potential (being the density-derivative of E_{xc}) in terms of explicit orbital derivatives of the implicit density functional [12, 13]:

$$v_{\mathrm{xc}}(\mathbf{r}) = \frac{\delta E_{\mathrm{xc}}[\rho]}{\delta \rho(\mathbf{r})} \tag{3.3}$$

$$= \sum_i \int \mathrm{d}\mathbf{r}' \int \mathrm{d}\mathbf{r}'' \frac{\delta E_{\mathrm{xc}}[\{\phi_i\}]}{\delta \phi_i(\mathbf{r}')} \frac{\delta \phi_i(\mathbf{r}')}{\delta v_s(\mathbf{r}'')} \frac{\delta v_s(\mathbf{r}'')}{\delta \rho(\mathbf{r})} + \mathrm{c.c.}, \tag{3.4}$$

which after some manipulation leads to a computationally accessible integral equation for the OEP,

$$\int \mathrm{d}\mathbf{r}' \; \chi_s(\mathbf{r}, \mathbf{r}') v_{\mathrm{xc}}(\mathbf{r}') = \Lambda(\mathbf{r}), \tag{3.5}$$

where χ_s, the noninteracting density response function, and Λ are both known explicitly in terms of the KS orbitals and orbital energies. In this form the OEP is the solution to a Fredholm integral equation of the first kind which, as has been noted

[76], is generally ill-posed. Various methods that project this equation into a finite space have been implemented [73, 74, 79].

A conceptually and computationally simpler approach is to minimize the OEP energy expression directly. To do so some useful form for the trial potential must be constructed. The direct OEP approach of Yang and Wu [48] does this by expanding the KS potential into a finite basis set $\{g_t(\mathbf{r})\}$ as

$$v_s(\mathbf{r}) = v(\mathbf{r}) + v_0(\mathbf{r}) + \sum_t b_t g_t(\mathbf{r}), \tag{3.6}$$

where v is the external potential of the system under consideration and v_0 a fixed reference potential. In this way the functional dependance of the energy upon the KS potential is transferred onto the coefficients $\{b_t\}$ and the problem of determining the ground state energy is expressed as an unconstrained minimization of the energy as a function of the $\{b_t\}$:

$$E_{N,v}^{\mathrm{OEP}} = \min_{\mathbf{b}} \langle \Phi(\mathbf{b}) | \hat{H}_v | \Phi(\mathbf{b}) \rangle. \tag{3.7}$$

The availability of the derivatives,

$$\begin{aligned} \frac{\partial E}{\partial b_t} &= \sum_i \int \mathrm{d}\mathbf{r}' \, \frac{\delta E}{\delta \phi_i(\mathbf{r})} \frac{\delta \phi_i(\mathbf{r})}{\delta v_s(\mathbf{r}')} \frac{\partial v_s(\mathbf{r}')}{\partial b_t} + \text{c.c.}, \\ &= \sum_i^{\mathrm{occ}} \sum_a^{\mathrm{virt}} \int \mathrm{d}\mathbf{r} \, \frac{\delta E}{\delta \phi_i(\mathbf{r})} \phi_a(\mathbf{r}) \frac{\langle \phi_a | g_t | \phi_i \rangle}{\epsilon_i - \epsilon_a} + \text{c.c.}, \end{aligned} \tag{3.8}$$

and of an approximate Hessian give rise to a direct and efficient iterative implementation of the OEP minimization statement based on a modified Newton method [80] detailed in the following section. The explicit orbital derivatives of the energy functional appearing in Eq. 3.8 are related to an effective Hamiltonian such that $\delta E / \delta \phi_i = \hat{H}_{\mathrm{eff}} \phi_i^*$ (for the EXX functional, $\hat{H}_{\mathrm{eff}}$ is simply the Fock operator expressed in terms of the KS orbitals). The above construction for the KS potential then yields

the exchange-correlation potential at convergence as

$$v_{\rm xc}(\mathbf{r}) = v_0(\mathbf{r}) - v_J(\mathbf{r}) + \sum_t b_t g_t(\mathbf{r}), \tag{3.9}$$

where v_J is the coulomb potential of the self consistent OEP density. The freedom associated in choosing the reference potential is often exploited so to enforce the correct asymptotic behavior of the exact exchange-correlation potential. We typically use the Fermi-Amaldi potential [81, 61, 82, 83] of a fixed density ρ_0,

$$v_0(\mathbf{r}) = \frac{N-1}{N} \int \mathrm{d}\mathbf{r}' \; \frac{\rho_0(\mathbf{r}')}{|\mathbf{r}-\mathbf{r}'|}, \tag{3.10}$$

although in those situations where the asymptotic correction is not desired the Coulomb potential of a reference density is typically employed. In addition, the size-consistency issue associated with the Fermi-Amaldi potential has also been addressed recently [83].

3.3 Computational Background

Our goal is to minimize the OEP energy as a function of the basis set expansion coefficients, $E(\mathbf{b})$, in a manner that ensures a physically meaningful potential and energy are obtained. The first derivative, $\nabla_{\mathbf{b}} E(\mathbf{b})$, is available from Eq. 3.8 as, too, are approximate and exact forms for the energy Hessian, $\mathbf{H} = \nabla^2_{\mathbf{b}} E(\mathbf{b})$. As such, a modified Newton method has been employed for the minimization [80]. In this way the potential is iterated as $\mathbf{b}_{n+1} = \mathbf{b}_n + \alpha \mathbf{p}$ where $\mathbf{p}$ is obtained from solving

$$\mathbf{H}(\mathbf{b}_n)\mathbf{p} = -\nabla E(\mathbf{b}_n) \tag{3.11}$$

and α is chosen to ensure the step size gives a sufficient decrease in the energy while ensuring global convergence. We typically use an approximate form for the Hessian

$$\mathbf{H}_{tu} \sim -\mathbf{X}_{tu} = \sum_i^{\rm occ} \sum_a^{\rm virt} \frac{\langle \phi_i | g_t | \phi_a \rangle \langle \phi_a | g_u | \phi_i \rangle}{\epsilon_i - \epsilon_a} + \text{c.c.}, \tag{3.12}$$

although the exact form is also available. This approximation is ideal, for it provides a globally positive definite expression that is physically related to the exact Hessian [80, 5]. We should note that the finite basis representation of the OEP problem can be expressed exactly as [80] $\mathbf{Xb} = \mathbf{c}$, where $\mathbf{X}$ is the approximate Hessian of Eq. 3.12. In this form the inverse nature of the problem and the fundamental significance of this Hessian, albeit approximate, is evident.

As we will see, the Hessian can be very ill-conditioned requiring some form of regularization to solve for a physically reasonable update. This has typically been accomplished using either a truncated singular value decomposition (TSVD) or Tikhonov regularization approach [80]. We will briefly consider only the TSVD in this chapter, where those eigenvectors of the Hessian corresponding to eigenvalues below some threshold, σ^*, are neglected when solving Eq. 3.11.

3.4 Regularized OEP

It has been well demonstrated that the finite basis OEP procedure fails when we have generated nonphysical potentials, and that the nonphysical behavior of these potentials has been observed as an excessively oscillatory behavior originating from the basis set expansion term of the potential (which we denote as $v_{\mathbf{b}}$) [67, 84]. As such, we define a regularized OEP energy functional as

$$\Omega_\lambda(\mathbf{b}) = E^{\mathrm{YW}}(\mathbf{b}) + \lambda||\nabla v_{\mathbf{b}}(\mathbf{r})||^2, \tag{3.13}$$

where $||\nabla v_{\mathbf{b}}(\mathbf{r})||^2 = 2\mathbf{b}^{\mathrm{T}}\mathbf{T}\mathbf{b}$, $\mathbf{T}$ is the kinetic energy integral matrix in the potential basis and $E^{\mathrm{YW}}(\mathbf{b})$ is the OEP energy calculated according to the Yang–Wu method. The energy derivatives with respect to the potential basis expansion coefficients are modified accordingly as $\nabla_{\mathbf{b}}\Omega_\lambda = \nabla_{\mathbf{b}}E^{\mathrm{YW}} + 4\lambda\mathbf{T}\mathbf{b}$ and $\nabla^2_{\mathbf{b}}\Omega_\lambda = \nabla^2_{\mathbf{b}}E^{\mathrm{YW}} + 4\lambda\mathbf{T}$. As the additional term present in the energy Hessian is (globally) positive definite we can use without modification the same Newton method for the minimization of

the regularized energy as we do the conventional OEP energy. The non-negative regularization parameter λ allows the energy functional to be supplemented with the smoothing term that drives the minimization to physical exchange-correlation potentials.

Of course, we do not know a-priori what value λ should take, nor is there a unique value for which it must obtain. Rather, some degree of subjectivity, arising from experience, must be introduced in to our reasoning. In this respect we emphasize that the regularization method we developed is not a penalty function method: There is simply no constraint upon what λ or $||\nabla v_{\mathbf{b}}(\mathbf{r})||$ must equal in our finite basis calculations.

With the introduction of λ we do not need to apply a separate regularization method to the approximate Hessian when solving for the update (Eq. 3.11). This is of particular significance: Unlike methods that use any form of regularization employing "cut-offs" – of which truncated SVD is one example – there is no ad hoc removal of information from the energy functional when solving for the OEP.

Our method of determining the optimal λ is motivated by the so called L-curve analysis [85] – which involves forming the curve of the smoothing norm against the energy relative to the HF energy (for the EXX functional) and is found to be useful when constructed in a log-log plot. We can obtain some insight to the possible structure of an L-curve in this setting by examining the derivative of the regularized energy functional with respect to the regularization parameter. Minimizing the regularized OEP functional for a given λ is equivalent to

$$\nabla_{\mathbf{b}} E^{\mathrm{YW}}(\mathbf{b}) + \lambda \nabla_{\mathbf{b}} ||\nabla v_{\mathbf{b}}(\mathbf{r})||^2 = 0 \tag{3.14}$$

which yields the regularized energy and potential for the specific λ at the minimizing potential specified by $\mathbf{b}^* : E(\lambda) = E^{\mathrm{YW}}(\mathbf{b}^*, \lambda),\ v_s(\lambda) = v_0 + v_{\mathrm{ext}} + v_{\mathbf{b}^*}(\lambda)$. The

derivative with respect to the regularization parameter follows as

$$\frac{\partial E}{\partial \lambda} = \nabla_{\mathbf{b}} E \cdot \frac{\partial \mathbf{b}}{\partial \lambda} = -\lambda \nabla_{\mathbf{b}} ||\nabla v_{\mathbf{b}}(\mathbf{r})||^2 \cdot \frac{\partial \mathbf{b}}{\partial \lambda}, \tag{3.15}$$

$$= -\lambda \frac{\partial ||\nabla v_{\mathbf{b}}(\mathbf{r})||^2}{\partial \lambda}. \tag{3.16}$$

When the condition $\partial ||\nabla v_{\mathbf{b}}(\mathbf{r})||^2 / \partial \lambda \neq 0$ holds we can express the derivative of the L-curve as [86]

$$\frac{\partial \ln ||\nabla v_{\mathbf{b}}(\mathbf{r})||^2}{\partial \ln \Delta E} = -\frac{\Delta E}{\lambda ||\nabla v_{\mathbf{b}}(\mathbf{r})||^2}. \tag{3.17}$$

From these expressions we can qualitatively interpret the three different structures observed for an L-curve as $\lambda \to 0$:

Structure A: $\partial ||\nabla v_{\mathbf{b}}(\mathbf{r})||^2 / \partial \lambda \sim 0$ for $\lambda \in [0, \lambda^*]$ with λ^* being significantly larger than 0, implying the L-curve flattens out in the limit of an unregularized solution. This is depicted in panel A of Fig. 3.1.

This is the ideal situation for computation. It signifies that we have chosen *balanced* orbital and potential basis sets and that, in fact, regularization was unnecessary for the best potential is that corresponding to $\lambda = 0$. We most often encounter such ideally balanced basis sets when using coinciding orbital quality contracted basis sets for the orbitals and potential. While the use of coinciding basis sets does not always result in such an ideal L-curve behavior (especially for very large basis sets and uncontracted basis sets), it is generally appropriate for TSVD regularization alone and as such is a commonly used choice for practical computations [87, 88]. Although little effort is required with such a choice, depending on the extent of contraction we may not have an ideal representation of the potential and instead have a larger basis set than what is needed if we were to use a *carefully* constructed uncontracted basis set.

Structure B: $\Delta E/||\nabla v_{\mathbf{b}}(\mathbf{r})||^2$, while small, remains finite ($\Delta E \neq 0$ and $||\nabla v_{\mathbf{b}}(\mathbf{r})||$ bounded) giving rise to a near-ideal L-curve as depicted in the panel B of Fig. 3.1.

While this situation indicates poorly balanced basis sets, with nonphysical potential obtained on the near-vertical portion of the L-curve, it is still favorable (in its ideal form) in that the optimal potential, and energy, are uniquely defined at the sharp corner of the L-curve. Moreover, if we are only interested in the total energy no regularization is required here. For most other quantities however, the unregularized potential will be unacceptable and the regularized potential would be required.

Structure C: ΔE tends to zero in some fashion leading to a unpredictable increase as depicted in the panel C of Fig. 3.1.

This, the least desirable case, necessitates an L-curve analysis to extract both physical potentials and energies. It is also the situation for which some ambiguity exists to where the optimal potential lies of the curve. There are two obvious points of interest – the point of maximum curvature of the L-curve [89], and the point of least change in the potential on the L-curve [78]. Extensive calculations have shown [84] that on the L-curve at the point of maximum curvature, nonphysical oscillations have already been introduced in to the potential, while the minimum derivative point yields excellent potentials. We will also consider the extent to which the OEP and orbitals satisfy rigorous relations derived from density scaling, which will be seen to yield excellent potentials corresponding to energies between the maximum curvature and minimum derivative points.

3.5 Results

All calculations were performed within a locally modified version of NWChem [90] using Cartesian Gaussian basis sets. Energies are converged to at least $10^{-10}E_{\mathrm{h}}$ with

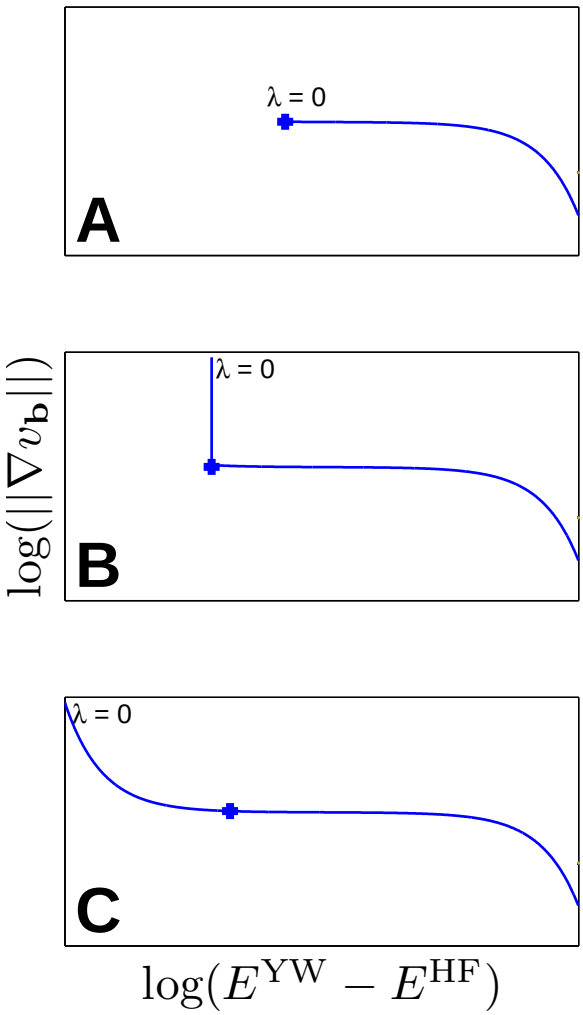

FIGURE 3.1: The three idealized forms of an L-curve. The position of the optimal potential, and their corresponding energies, for each class of curves are denoted with a cross. Panels A and B provide an obvious and well defined point for selecting the optimal potential and energy while panel C requires some judicious choice as described within the text. We employ $||\nabla v_{\mathbf{b}}(\mathbf{r})||$ as the smoothness measure of our potentials, and $E^{\mathrm{YW}} - E^{\mathrm{HF}}$ (or $E^{\mathrm{YW}} - E^{\mathrm{DFT}}$ for functionals other than EXX) as the energy measure, although these choices are not unique.

corresponding OEP energy gradients, $||\partial E^{\mathrm{OEP}}/\partial \mathbf{b}||_1$, typically no greater than 10^{-6}.

The majority of our OEP calculations employ the EXX energy functional, however it is insightful to use an explicit density functional so that we can judge the quality of our finite-basis OEP's by comparison with the potentials generated from

a conventional DFT calculation. With this in mind we will consider several OEP calculations employing the LDA (SVWN5) functional. Such calculations do not use the Fermi-Amaldi form of the reference potential but rather a Coulomb reference potential so as to not correct the exponential asymptotic behavior inherent to the LDA potential. This necessitates shifting the resultant OEP's by a constant so their HOMO energy coincides with that of a conventional DFT LDA calculation to allow for direct comparison. EXX OEP calculations do employ the Fermi-Amaldi potential and as such EXX OEP's do not need to be shifted.

We will use the notation "ao basis / xc basis (λ)" to describe a calculation performed with the specified orbital and potential basis sets and with a regularization parameter of λ. For example, using the cc-pVTZ basis to describe the orbitals and cc-pV5Z basis to describe the potential with a regularization parameter of 10^{-6} would be written as cc-pVTZ/cc-pV5Z (10^{-6}).

3.5.1 Extracting potentials from the L-curve

For demonstration purposes, we consider a linear FC_2Cl molecule (bond lengths: F-C 1.26850Å, C-C 1.17777Å, C-Cl 1.65675Å). As we do not know the exchange potential for this molecule, we use the LDA (SVWN5) [91, 9] potential generated from a conventional DFT calculation as a reference and perform OEP calculations utilizing the LDA energy functional to judge our results. We will use the cc-pVDZ [92] basis for the orbitals and the Partridge Uncontracted 3 [93] basis (denoted hereafter as PU3) for the potential. This combination provides an extremely unbalanced pair to highlight the robustness of our approach.

Fig. 3.2 displays the LDA OEPs obtained using the conventional TSVD approach for several values of the SVD cutoff employed, together with the LDA potential obtained from a conventional DFT calculation. No matter what value for the SVD cutoff, σ^*, is used, we can not obtain physically reasonable potentials. We can how-

ever isolate the irregularities to regions near the nuclei. Using larger values of the SVD cutoff drastically effects the convergence we can obtain, and as such this approach is completely unacceptable for this absurdly unbalanced choice of orbital and potential basis sets. On the other hand, our regularized OEP functional together with a L-curve analysis yields potentials in excellent agreement with the LDA potential obtained from a conventional DFT calculation. Fig. 3.3 shows the L-curve together with the reciprocal of the L-curve derivative as given by Eq. 3.17. The optimal potential, as defined by the minimal slope of the L-curve, occurs at ($\lambda = 3.32 \times 10^{-6}$), which together with a potential near the point of maximum curvature of the L-curve ($\lambda = 1 \times 10^{-8}$) are shown in Fig. 3.4. Discrepancies between the potential at the point of minimum slope of the L-curve and the LDA potential only occur at the nuclei, a relic of the potential basis set, regularizing norm, and accuracy in λ^*, that we have employed.

From this simple example we have seen that firstly, the TSVD approach is not guaranteed to yield acceptable results (although we have to consider unbalanced basis sets for this to happen), and secondly that a high quality potential can be extracted from the L-curve at the point of minimal slope - but not the point of maximum curvature.

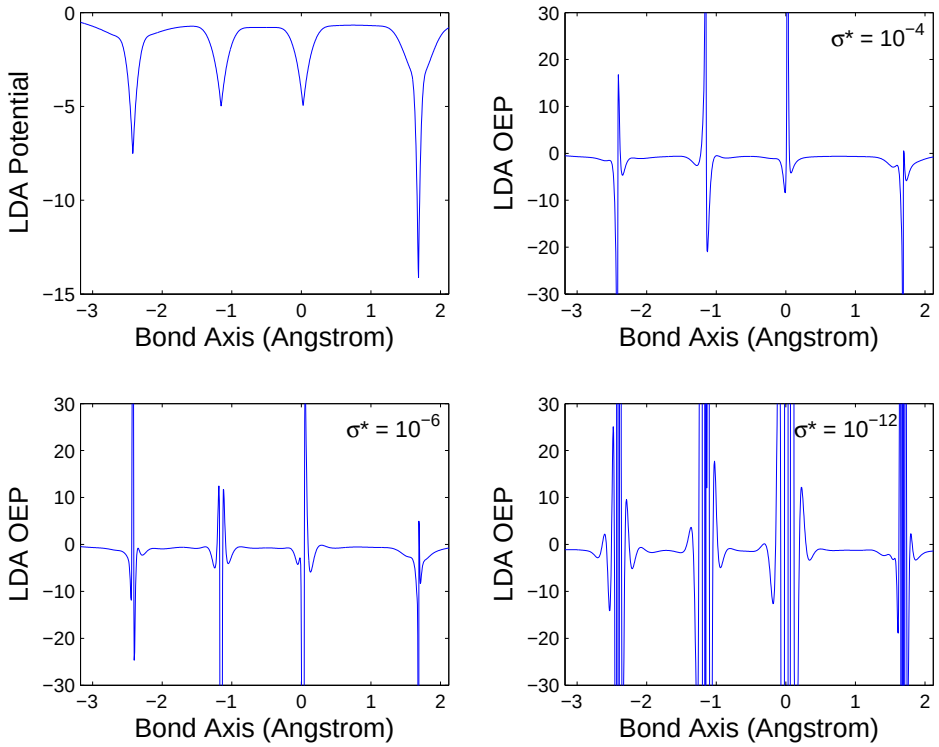

FIGURE 3.2: LDA OEP's obtained from the conventional TSVD regularization approach for different values of the SVD cutoff (σ^*) in our FC_2Cl example. Also shown is the LDA potential (upper left) obtained from a conventional DFT calculation. This demonstrates that, for this unbalanced combination of basis sets, there is no value of the cutoff which yields sensible potentials – further increasing σ^* results in unacceptable convergence.

3.5.2 Argon atom – comparison with grid-based OEP results

We now move on to examining the exact-exchange energies the L-curve approach generates. We first consider calculations upon an argon atom for which grid-based OEP calculations are available for comparison. These provide the most accurate OEP results when performed carefully so to ensure convergence and balance between the orbital and potential grids. We employ the Partridge Uncontracted 3 basis set for the orbitals as is often seen in the literature [73, 48, 94], and an even tempered potential basis set of s-type Gaussians with exponents $0.01 \times 2^n, 0 \leq n \leq 25$ (denoted as G26).

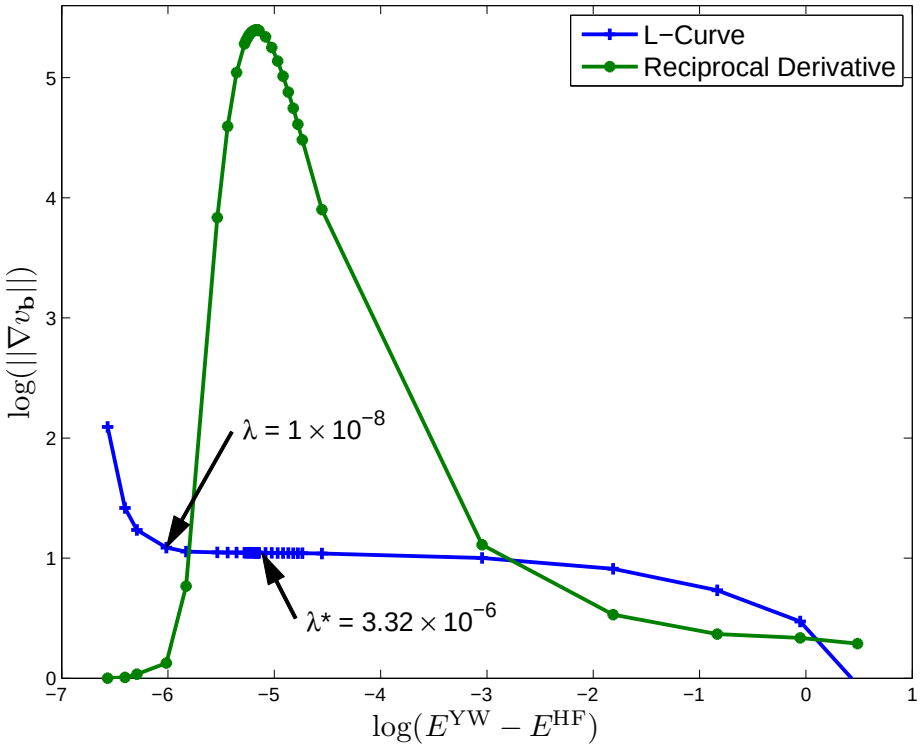

FIGURE 3.3: L-curve and its derivative for our FC_2Cl example. The point of minimum derivative is labeled as λ^* and a point closer to the maximum curvature is also shown. The potentials corresponding to these two values are shown in Fig. 3.4

Fig. 3.5 shows the L-curve for this combination of basis sets. As is typical with the use of large uncontracted orbital basis sets, the L-curve displays an ideal form with a well defined corner, and as such, an obvious choice for the optimal potential and energy. The generation of nonphysical potentials (those on the vertical portion of the L-curve) have essentially and same energy. This type of behavior can be highly misleading when one considers only the total energy as an indicator of the quality of the calculation and we believe many of the early finite basis set OEP calculations, while yielding acceptable total energies, suffered from poor potentials owing to this behavior.

The optimal choice of potential corresponds to $\lambda = 2.10 \times 10^{-5}$. This potential, as seen from the insert of Fig. 3.5, agrees very well with the grid-based potential and

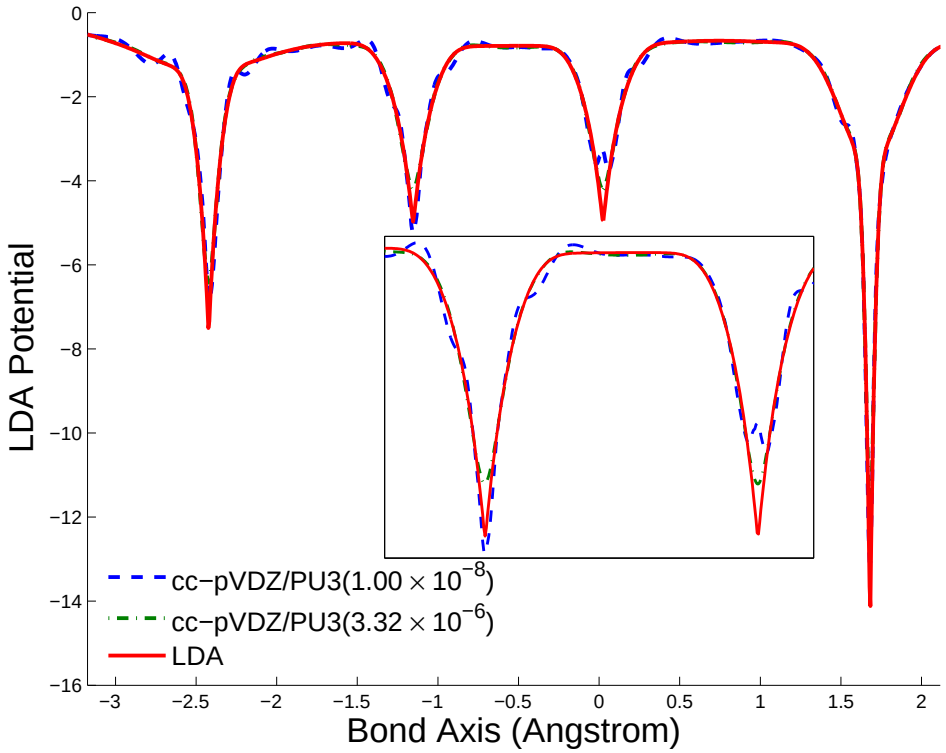

FIGURE 3.4: Optimal potential (corresponding to the minimum derivative in Fig. 3.3) and one potential near the maximum curvature together with the LDA potential obtained from a conventional DFT calculation for our FC_2Cl example. Insert: magnified portion of the potentials between the two carbon atoms.

as seen in Table 3.1, yields an energy of -526.8123 E_h (as compared to the grid-based value of -526.8122 E_h). Notably, the orbital energies our potential generates have significant discrepancies from the grid calculation values. By considering different values of λ we have found that a much better agreement in the orbital energies can be obtained with $\lambda = 1.74 \times 10^{-6}$ (as shown in Table 3.1). However for this smaller value of λ the potential differs significantly from the grid potential, particulary in the regions of the shell maxima, as well as having numerous small nonphysical bumps (see the insert of Fig. 3.5). This is significant as previously reported calculations on the argon atom with this orbital basis set have yielded much better agreement with the grid-derived orbital energies than our optimal potential does. In particular the

calculations of Ivanov et al. [94] which they denote as EXX-χ (and are reproduced in the final column of Table 3.1) obtain a near perfect agreement with the grid spectrum, although the details of their corresponding exchange potentials were not presented. The recent study of Kollmar and Filatov [95] suggests such an ideal agreement with the grid values with this orbital basis (20s/15p) is highly unlikely, and the deviations we observe with our optimal potential are, in fact, in good agreement with their observations.

For comparison to the TSVD approach commonly used, the final column of Table

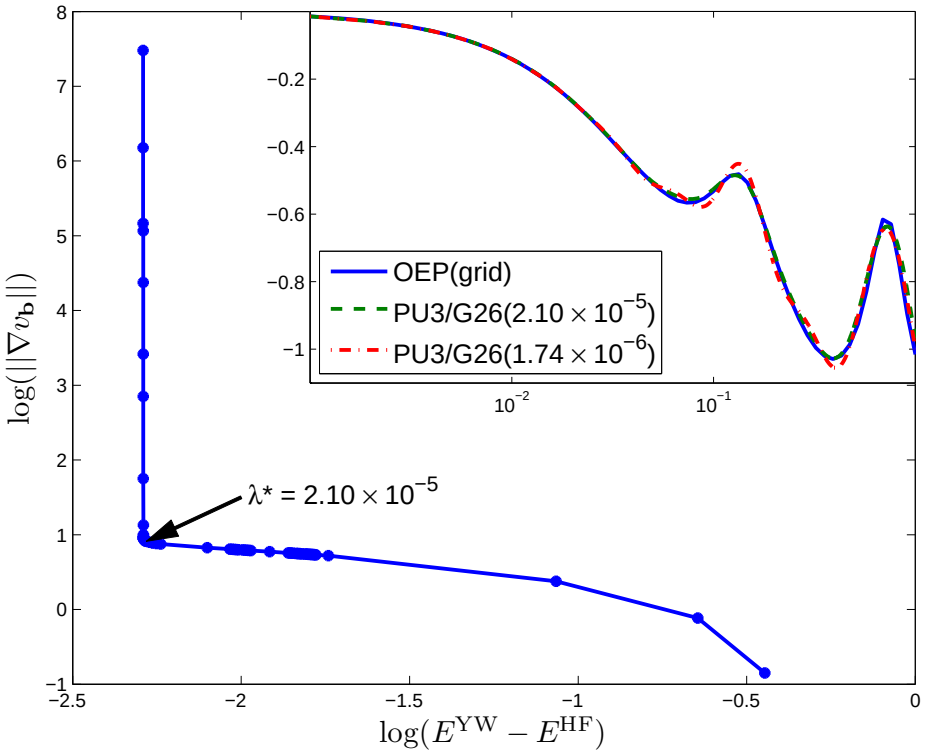

FIGURE 3.5: L-curve for an argon atom with the Partridge Uncontracted 3 (PU3) orbital basis set and a 26 term even tempered (G26) potential basis set as described within the text. The insert shows the radially weighted exchange potential ($rv_x(r)$) derived from a grid-based calculation, together with the optimal potential ($\lambda^* = 2.10 \times 10^{-5}$) and a slightly nonphysical potential ($\lambda = 1.74 \times 10^{-6}$) that yields orbital energies in much better agreement with the grid-based OEP values than does the optimal choice.

3.1 displays the results of a calculation using a SVD cutoff of $\sigma = 1 \times 10^{-6}$ – a value that has often been used de-facto. This yields significant discrepancies in both the total energy and orbital energies, together with a very oscillatory potential. Increasing the SVD cutoff does yield improvements but the particular choice of σ^* is a delicate task owing to the dramatic range of exponents this basis set contains, and thus the ease at which poor potentials can be generated.

Table 3.1: Comparison of regularized OEP energies with Hartree-Fock and grid based OEP energies for an argon atom represented by the Partridge-3 orbital basis set the 26 s-type Gaussian potential basis set described in a text. All energies are in hartree. Two non-zero values of the regularization parameter are presented: $\lambda = 2.10 \times 10^{-6}$ is the optimal value whereas $\lambda = 1.74 \times 10^{-6}$ yields better agreement with the orbital energies obtained from a grid-based approach but a poor potential as shown in Fig. 3.5.

	HF	OEP					
		grid	$\lambda = 0$	$\lambda = 2.10 \times 10^{-5}$	$\lambda = 1.74 \times 10^{-6}$	$\sigma = 1.00 \times 10^{-6}$	Ivanov *et al.* [94]
Energy	-526.8175	-526.8122	-526.8124	-526.8123	-526.8124	-526.8124	-526.8123
$1s$	-118.6103	-114.4524	-114.4468	-114.3948	-114.4452	-114.2934	-114.4514
$2s$	-12.3221	-11.1534	-11.1518	-11.1283	-11.1533	-10.9993	-11.1539
$2p$	-9.5715	-8.7339	-8.7318	-8.7127	-8.7339	-8.5794	-8.7343
$3s$	-1.2773	-1.0993	-1.0998	-1.0756	-1.0994	-0.9460	-1.0993
$3p$	-0.5910	-0.5908	-0.5908	-0.5676	-0.5909	-0.4374	-0.5908
$\|\|\nabla v_{\mathbf{b}}\|\|$	–	–	1.50×10^8	8.15×10^2	8.98×10^2	1.33×10^3	–

3.5.3 N_2 and CO molecules – testing the exchange energy virial relation as a measure for choosing the optimal potential

Here we wish to introduce more physical insight for the selection of the optimal OEP on the L-curve by incorporating some dependance upon the KS orbitals and density. In this respect, particularly useful quantities are exact relations derived from density scaling such as [96, 97]

$$E_x[\rho, v_x] = \int \mathrm{d}\mathbf{r}\ v_x(\mathbf{r})\Big(3\rho(\mathbf{r}) + \mathbf{r}\cdot\nabla\rho(\mathbf{r})\Big), \tag{3.18}$$

which holds exactly in the complete basis set limit. We shall use the extent to which this exchange energy virial relation is satisfied in our finite basis calculations as a method of extracting the optimal value of the regularization parameter from the L-curve. Specifically we consider $\Delta[v_x] = (E_x^{\mathrm{direct}}[\{\phi_i\}] - E_x[\rho, v_x])^2$ where E_x^{direct} is the energy contribution obtained directly from the orbital-dependant exchange functional, and $E_x[\rho]$ is the right-hand side of Eq. 3.18. Used in this way we introduce a deeper physical reasoning into the selection of λ^*, and in itself this expression is somewhat more useful for judging the quality of our potentials than the results of grid-based calculations (which are only available for atoms) where we must approach the basis set limit for any meaningful comparisons to be made.

Some care does need to be taken when using this quantity as a measure of the quality of an OEP for, while it holds exactly for the exact potential, it can also be very well satisfied for (finite basis) potentials which display nonphysical behavior. When used in combination with the OEP functional regularized with the smoothing norm we can however be assured of not being mislead in this way. One may be tempted to replace the smoothing norm as a regularization measure with the extent to which Eq. 3.18 is satisfied within the regularized OEP functional itself. While this does extremely well to force the virial relation to be satisfied, it does not help to generate physical potentials.

This measure is particularly useful for those combinations of orbital and potential basis sets that give rise to an L-curve that lack a well defined optimum potential and energy. To facilitate a clear example we will specifically chose basis sets that give rise to such a poor L-curve. For N_2 and CO we employ the (contracted) cc-pVTZ orbital basis, and the PU3 potential basis set and present the L-curve, its derivative, and the extent to which Eq. 3.18 is satisfied as measured by $\Delta[v_x]$. These are shown in Figs. 3.6 and 3.7, together with numerical values of various quantities in Table 3.2.

The two different choices for selecting an optimal potential – the minimal slope and the satisfaction of Eq. 3.18 – agree very well with regards to λ, and the two

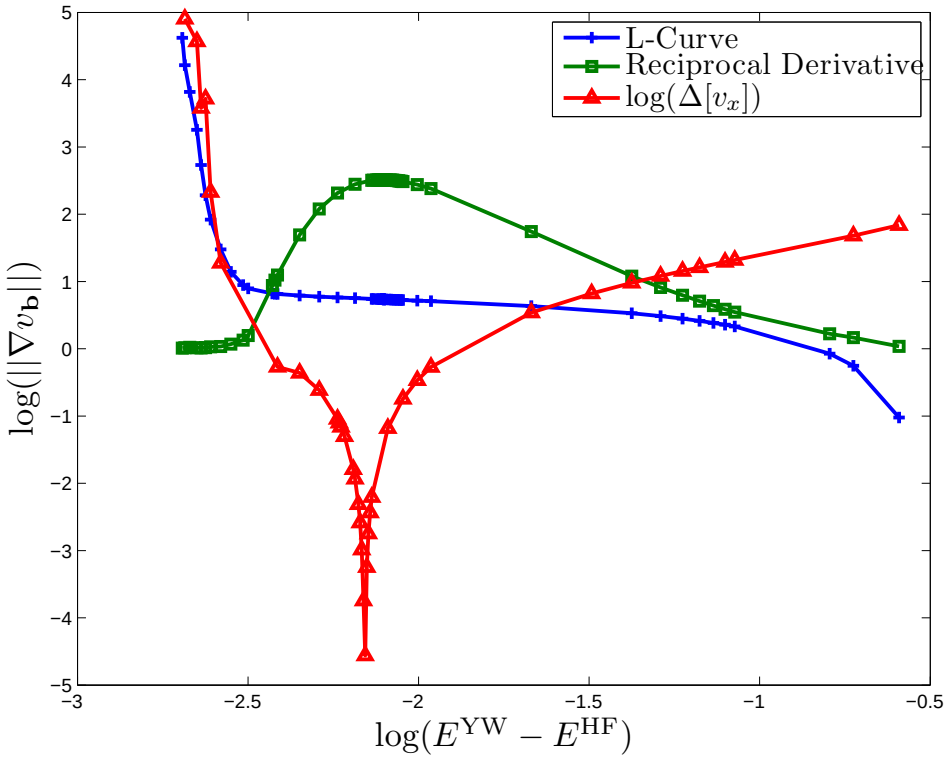

FIGURE 3.6: The L-curve, its derivative, and the extent to which the exchange energy virial relation is satisfied for the nitrogen molecule. The orbital basis set is cc-pVTZ, and for the potential it is the Partridge Uncontracted 3 basis set.

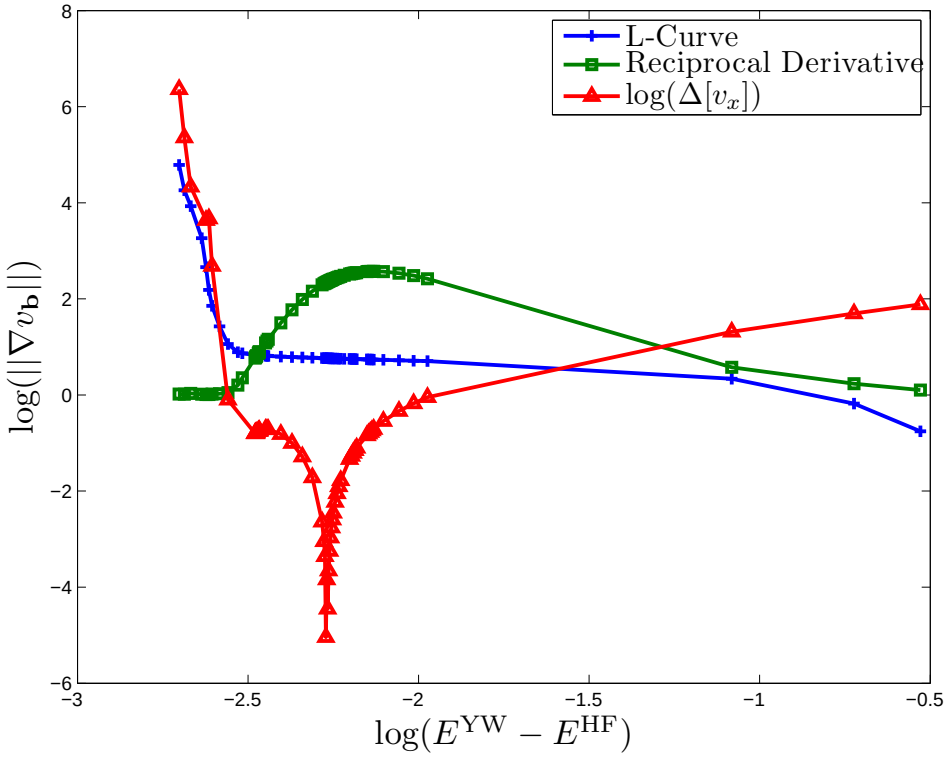

FIGURE 3.7: The L-curve, its derivative, and the extent to which the exchange energy scaling relation is satisfied for the carbon monoxide molecule. The orbital basis set is cc-pVTZ, and for the potential it is the Partridge Uncontracted 3 basis set.

exchange potentials agree very well. The only obvious differences between the potentials occur at the nuclei and internuclear maxima as seen in Fig. 3.8 for CO. The total energy is fairly insensitive to λ near the optimal value for both choices. As shown in Table 3.2, λ accurate to four significant figures results in OEP energies stable to beyond the micro-Hartree level. Further, the scaling relation always selects a smaller optimal value of λ, and hence lower energy. Clearly this implies that the derivative condition is not optimal.

In our finite basis representation of the exchange-correlation OEP, the separation of exchange and correlation terms is not possible. As such Eq. 3.18 is only useful when using the EXX functional. A possibility for general exchange-correlation

Table 3.2: Values of the optimal regularization parameter and corresponding energy as determined by the minimum derivative condition and the satisfaction of the exchange virial relation corresponding to Figs. 3.6 and 3.7. ΔE is the mean of $E(\lambda^* \pm 1 \times 10^{-7})$ and as such is a measure of the sensitivity of the energy to the regularization parameter in the vicinity of λ^*. Energies in hartrees.

	N_2	CO
λ^*_{deriv}	6.690×10^{-4}	6.478×10^{-4}
$\lambda^*_{\text{virial}}$	5.572×10^{-4}	3.767×10^{-4}
E_{deriv}	-108.976 193 544	-112.773 455 554
E_{virial}	-108.977 102 968	-112.775 509 173
ΔE_{deriv}	8.41×10^{-7}	8.28×10^{-7}
ΔE_{virial}	7.84×10^{-7}	6.80×10^{-7}
$\|\|\nabla v_{\mathbf{b}}\|\|_{\text{deriv}}$	5.43	5.44
$\|\|\nabla v_{\mathbf{b}}\|\|_{\text{virial}}$	5.57	5.80

functionals is to use the similarly scaling-derived result for the KS kinetic energy [96, 97]

$$T_s[\rho] = -\frac{1}{2}\int \mathrm{d}\mathbf{r}\; v_s(\mathbf{r})\left(3\rho(\mathbf{r}) + \mathbf{r}\cdot\nabla\rho(\mathbf{r})\right), \tag{3.19}$$

although we will restrict ourselves to the EXX functional and the exchange energy virial relation here.

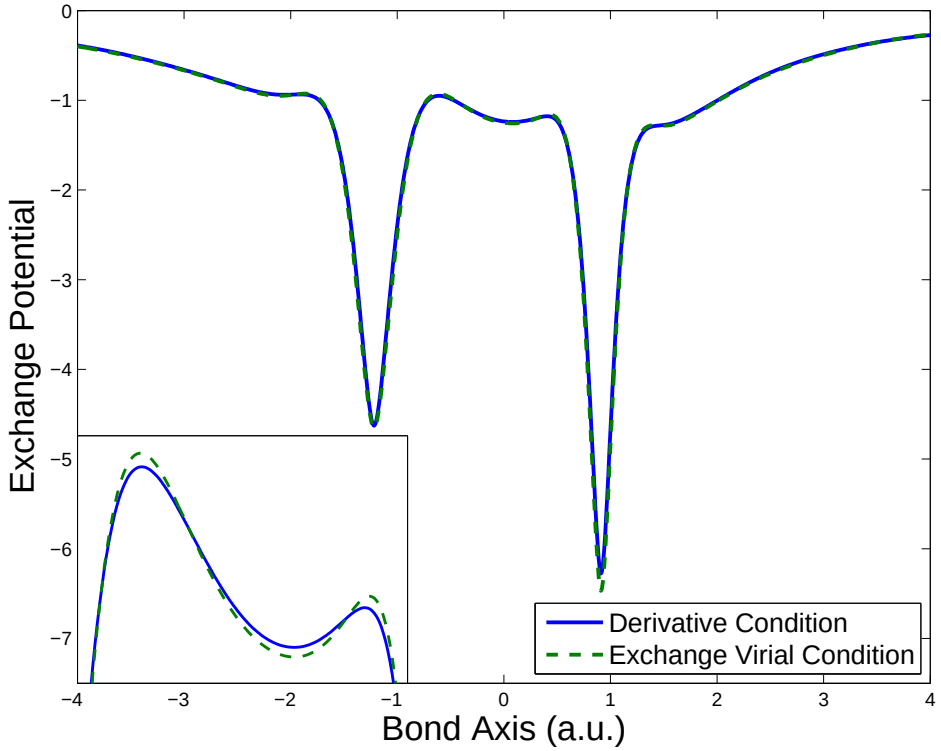

FIGURE 3.8: The exchange potentials of CO obtained from the L-curve analysis corresponding to Fig. 3.7 for the two choices of optimal λ: the point of minimum derivative of the L-curve, and the point of maximal satisfaction of the exchange virial relation. The insert enlarges the internuclear region.

3.5.4 Varying the potential basis set

Typically we will be given an orbital basis set to work with and will need to select a potential basis set. In terms of the L-curve, this ideally involves increasing the cardinality of the potential basis set until the rise of the L-curve can not be further decreased. Fig. 3.9 shows such a situation for the nitrogen molecule represented in an uncontracted cc-pVTZ orbital basis set. For the present purposes, we consider the progression of Partridge Uncontracted 1, 2, and 3 potential basis sets together with uncontracted correlation consistent polarized valence triple-, quadruple-, and quintuple-zeta basis sets. The L-curves of all potential basis sets coincide exactly for large, nonphysical values of λ. It is clear to see that PU1 rises well before PU2

and PU3 and u-cc-pVTZ (denoted as uTZ hereafter). Despite the smaller dimension of the uTZ basis set, its behavior is significantly different from the PUn basis sets as λ approaches zero. There is not the dramatic rise associated with the generation of oscillatory potentials, and the OEP energy is significantly lower. We see this behavior as an exemplification of the concept of balanced orbital and potential basis sets. In this case the unbalance of the Partridge basis sets can be seen to be obvious simply by considering the largest exponents of the Gaussians comprising these basis sets: 11420 for uTZ and greater than 10^6 for PU3. For large values of λ (that is, smooth potentials) the tight functions of the PU3 basis contribute very little to the finite basis representation of the exchange potential, thereby decreasing the effective cardinality of the basis set. As λ approaches zero however, these functions play a

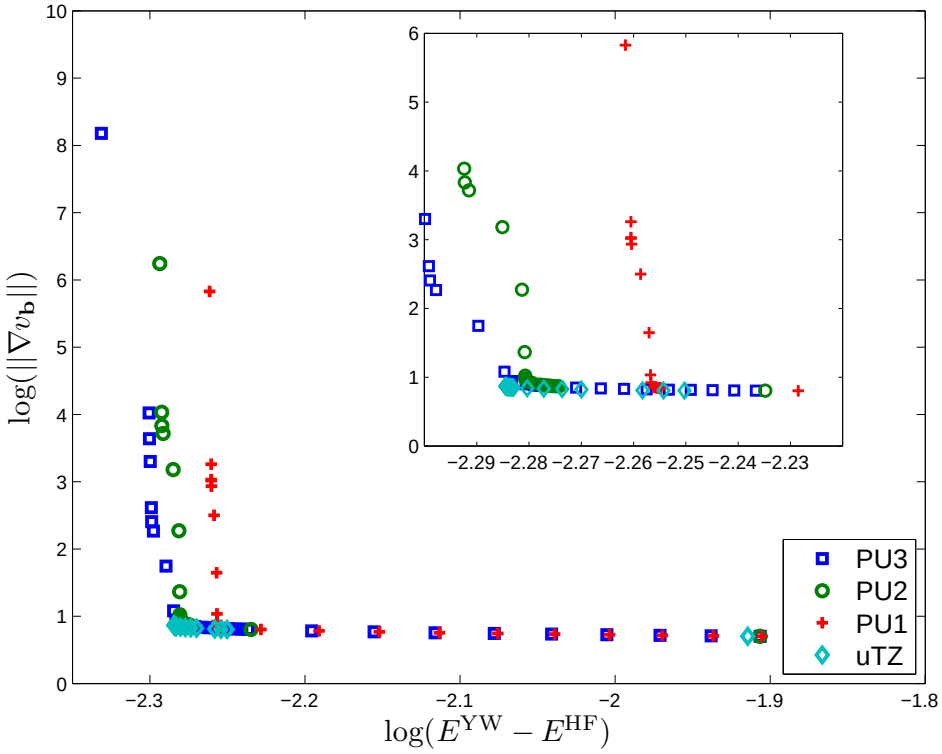

FIGURE 3.9: L-curves for a nitrogen molecule with an uncontracted cc-pVTZ orbital basis set and four different potential basis sets as described in the text.

significant role in the basis set introducing unpredictable nonphysical oscillations near the nuclei. The regularized OEP functional is able to balance these effects to yield physical potentials at the expense of a higher total energy than the inherently balanced uTZ basis set.

The extent of satisfaction of the exchange identity is shown in Fig. 3.10 for these potential basis sets. Quite dramatically, in the case of coinciding orbital and potential basis sets, the relation is satisfied to several orders of magnitude better than for all the others combinations, including the larger uQZ (of which uTZ is not a subset). Despite this, the uQZ OEP energy is the lowest - a case in point where the degree to which the virial relation is satisfied can not be used as an absolute measure of finite basis OEP's.

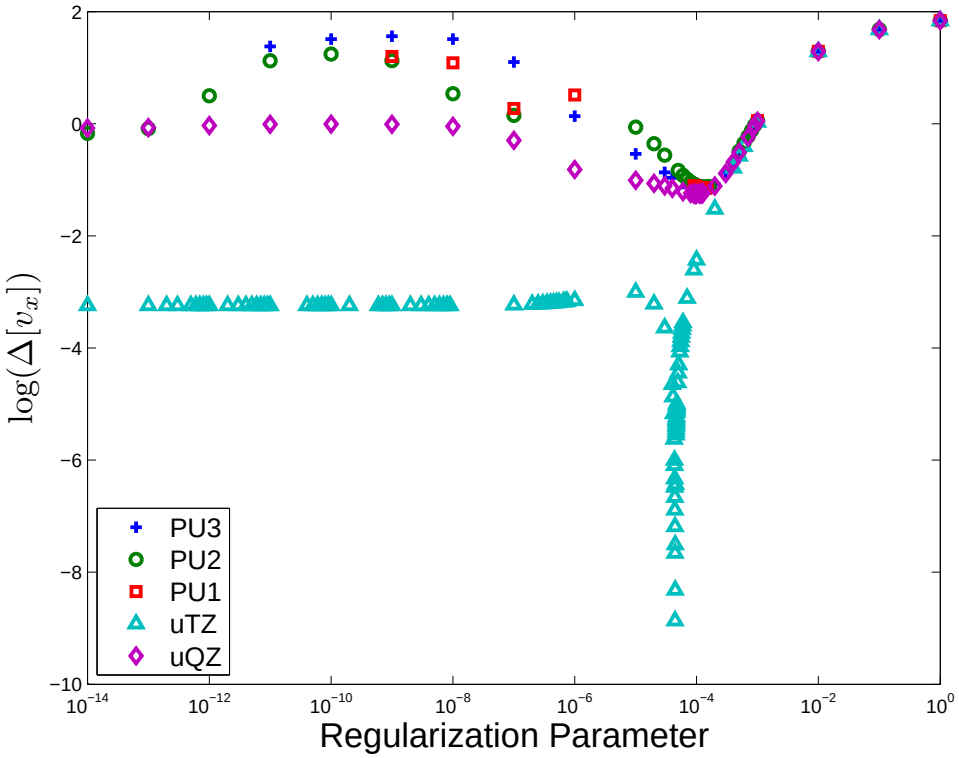

FIGURE 3.10: The extent to which the exchange energy virial relation is satisfied, as measured by $\Delta[v_x]$, as a function of the regularization parameter.

From Table 3.3, we see our HOMO energies are significantly smaller (and closer to the experimental ionization energy) than those of Ivanov *et al.* [94]. To see how the HOMO energy behaves as a function of the regularization parameter we present Fig. 3.11. All basis sets yield essentially identical L-curve derived HOMO energies for λ above 5×10^{-5}. The optimal λ for the uTZ/uTZ calculation is displayed as a vertical line in the figure and is seen to correspond to the structure appearing as a local minima (at 14.80 eV) that all the potential basis sets give rise to and which lies close to the experimental ionization energy (15.58 eV). For λ in this vicinity there is little variation in the HOMO energy for the regularized OEP functional calculations – a significant advantage over the TSVD approache which is well known to depend strongly on the cutoff used. In this case the TSVD regularization approach yields similar values in the vicinity of the optimal L-curve derived regularization parameter, although its variation is somewhat erratic. For smaller values of λ the HOMO energy behaves unpredictably, albeit in a smooth fashion for the regularized functional. The dashed horizontal line marks the HOMO energy found by Ivanov *et al.* (17.16 eV) [94], which coincidentally agrees fairly well with a TSVD calculation with cutoff of 10^{-6}.

Table 3.3: L-curve determined regularized OEP energies for N_2. Orbital basis set is that of uncontracted cc-pVTZ, while the potential basis set is varied as indicated. PUn denotes the Partridge Uncontracted basis sets. λ^* refers to the optimal value of the regularization parameter as determined by the exchange energy virial relation condition. Total energies are in units of mE_h relative to the Hartree-Fock energy of -108.984 681 E_h, and orbital energies are in eV. The experimental ionization energy is 15.58 eV. For the results of Ivanov *et al.*, we take the results denoted as EXX-χ of Table III in S. Ivanov, S. Hirata, and R. J. Bartlett. J. Chem. Phys., 116:1269, 2002, but note that this is only one of the approaches they proposed

	PU3	PU2	PU1	cc-pV5Z	cc-pVQZ	cc-pVTZ	Ivanov *et al.*
λ^*	1.27×10^{-4}	1.25×10^{-4}	1.11×10^{-4}	1.097×10^{-4}	9.98×10^{-5}	4.44×10^{-5}	–
$\|\|\nabla v_\mathbf{b}\|\|$	6.27	6.27	6.31	6.40	6.43	6.67	–
$E(\lambda^*)$	5.95	5.96	5.96	5.25	5.21	5.34	5.20
$E(\lambda = 0)$	5.01	5.05	5.49	4.06	4.38	5.19	–
$E_{\mathrm{HOMO}-5}$	-386.73	-386.61	-386.90	-386.67	-386.73	-387.02	-390.65
$E_{\mathrm{HOMO}-4}$	-386.70	-386.58	-386.86	-386.63	-386.69	-386.98	-390.62
$E_{\mathrm{HOMO}-3}$	-33.13	-33.03	-33.11	-33.06	-33.02	-32.62	-35.58
$E_{\mathrm{HOMO}-2}$	-17.86	-17.75	-17.86	-17.68	-17.64	-17.27	-20.23
$E_{\mathrm{HOMO}-1}$	-15.84	-15.73	-15.85	-15.59	-15.55	-15.19	-18.12
E_{HOMO}	-14.77	-14.67	-14.74	-14.72	-14.68	-14.23	-17.16
$E_{\mathrm{HOMO}+1}$	-5.67	-5.56	-5.68	-5.33	-5.28	-4.97	-7.91
$E_{\mathrm{HOMO}+2}$	2.08	2.20	2.07	2.18	2.23	2.71	0.26

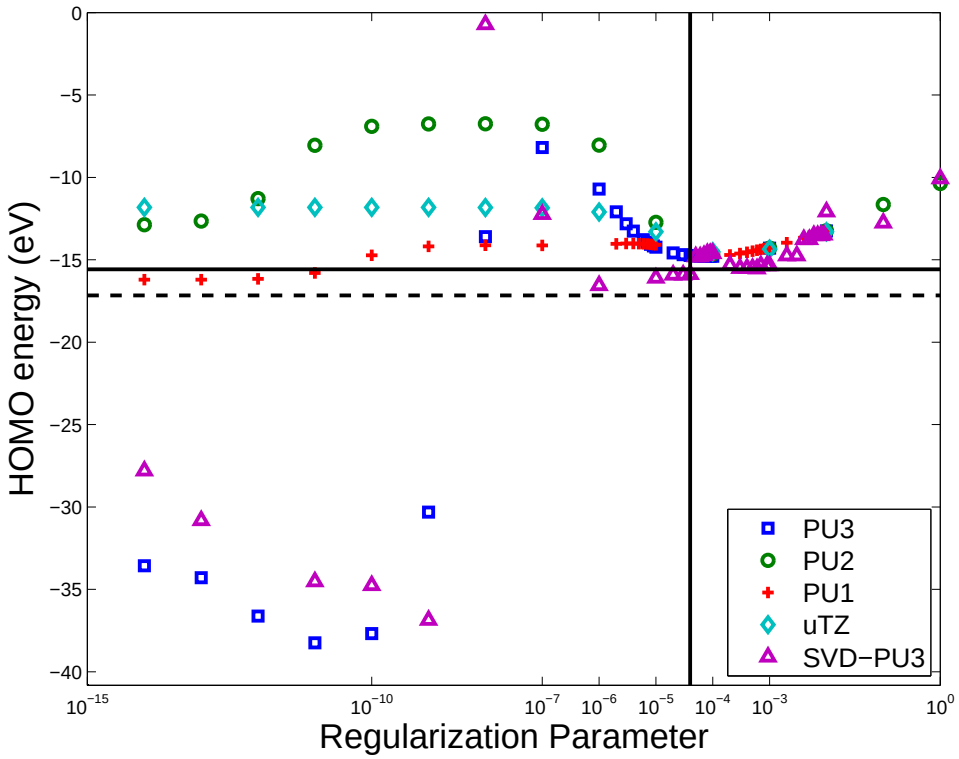

FIGURE 3.11: The HOMO energy for a nitrogen molecule as a function of the regularization parameter with four different potential basis sets. SVD-PU3 denotes calculations performed with the TSVD-regularization approach, rather than with the regularized OEP functional. The vertical line marks the optimal regularization parameter for the uTZ/uTZ calculation. The solid horizontal line marks the experimental ionization energy. The dashed horizontal line marks the HOMO energy obtained by Ivanov *et al.*(EXX $-\chi$).

3.5.5 Final examples

Finally we present ground-state EXX OEP energies and orbital energies for several molecules performed with a large orbital basis set. We hope that this will be useful for comparing different approaches for obtaining OEP energies with finite basis set. We employ the *spdf*-aug-cc-pV5Z basis set for the orbitals and the uncontracted *spdf*-aug-cc-pV6Z potential basis set. For the optimal value of the regularization parameter we use the extent to which the exchange energy virial relation is satisfied as described above. Our numerical values are shown in Table 3.4. We also compare the HOMO energies of these calculations with various other finite basis set approaches to the OEP problem in Table 3.5. One must be particulary careful when interpreting this table with regard to comparing different OEP methods as different basis sets, and possibly geometries, are used. On the other hand, Heßelmann *et al.* [69] have presented results for the HOMO energies in double- through quintuple-zeta basis sets and observed very little, if any, dependence of the HOMO energy on the basis set.

Table 3.4: OEP energies (in mE_h relative to the corresponding HF energy) and orbital energies (in eV) for a selection of molecules. We use the *spdf*-aug-cc-pV5Z basis set for the orbitals and the uncontracted *spdf*-aug-cc-pV6Z basis set for the exchange potential. λ is calculated to four significant figures, resulting in energies being accurate to at least the μE_h level. Geometries employed are C-O = 1.128 Å; N-N = 1.098 Å; O-O = 1.207 Å; F-F = 1.412 Å. The values of λ^* are CO: 1.1474×10^{-4}; N_2: 1.213×10^{-4}; O_2: 1.497×10^{-4}; F_2: 1.347×10^{-4}.

	N_2	CO	O_2	F_2
E^EXX	5.976	5.747	8.803	9.371
$E_\mathrm{HOMO-4}$	-14.2343	-10.1787	-0.9429	-1.5053
$E_\mathrm{HOMO-3}$	-1.2458	-1.2904	-0.7008	-1.2794
$E_\mathrm{HOMO-2}$	-0.6830	-0.7187	-0.6796	-0.7976
$E_\mathrm{HOMO-1}$	-0.6075	-0.6245	-0.6746	-0.7307
E_HOMO	-0.5736	-0.5141	-0.4218	-0.6088
$E_\mathrm{HOMO+1}$	-0.2335	-0.2311	-0.4036	-0.4084

Table 3.5: Comparison of our HOMO orbital energies with experimental ionization energies and other OEP approaches. All energies are in eV. Note that we are comparing calculations performed with different orbital basis sets and, in some cases, geometries.

Molecule	This Work	Ivanov *et al.*[73]	Görling [74]	Yang–Wu [48]	Hesselmann *et al.*[69]	HF	Experiment [98]
CO	13.99	15.03	14.1	13.67	15.0	15.10	14.01
N_2	15.61	17.16	15.5	14.05	–	16.71	15.58
O_2	11.48	–	13.6	–	–	17.78	12.07
H_2O	13.58	13.71	13.7	12.44	13.85	13.89	12.62
F_2	16.56	–	14.5	13.79	–	18.15	15.70

3.6 Concluding remarks

The concerns that have recently been raised relating to the viability of finite-basis set OEP methods have lead to several approaches to control the now well known numerical issues originating from the typically ill-posed nature of the OEP approach. While many of these approaches focus on restricting the orbital or potential basis sets based upon some preconception of what constitutes balanced combinations, we have shown how physically meaningful OEP calculations can be carried out for any arbitrary combination of orbital and potential basis sets. Our regularized OEP functional together with the L-curve analysis for determining the optimal regularization parameter has been shown to produce potentials of excellent quality. This approach explicitly introduces the regularization via a weighting term for the smoothness measure of the potential in the energy functional. We have introduced a physically meaningful condition for selecting the optimal value of λ by considering the exchange energy virial relation along the L-curve itself. Using this dual approach of the regularized functional and L-curve analysis we have approached the unbalanced OEP problem in a most sensible way given its ill-posed nature. That is, the problem must be first formulated in a well-posed manner and then solved to yield an approximate solution to the original ill-posed equations. Our results show that this approach is very successful in generating high-quality potentials and energies.

The shape of the L-curve in our approach also provides an excellent gauge on whether the potential and orbital basis sets are balanced, and thus on how to choose potential basis sets systematically.

In those situations where the basis sets are so balanced to render the problem (nearly) well-posed, we have much more freedom in how to solve for the OEP. In particular the TSVD regularization method that is widely employed provides a fast and stable method for such calculations.

4

Size Extensivity of the Direct Optimized Effective Potential Method[1]

4.1 Introduction

We now investigate a computational issue of the direct optimized effective potential procedure of Yang and Wu – a possible lack of size extensivity. Unlike the issues of ill-posedness, this aspect is not inherent to OEP but rather to specific implementations.

In molecular OEP applications there will be many situations where it is essential that size extensitivity – linear scaling of the energy with system size – is maintained so to allow for the calculation of meaningful relative energies. In the Yang–Wu direct OEP approach, the size extensitivity of our implementation depends on the choice of reference potential that is used to aid in basis set convergence. This reference potential can be utilized to ensure other desirable properties of the solution. In particular, a common choice enforces the correct asymptotic behavior of the exact exchange-correlation potential at the expense of having a non-size extensive method. A correct asymptotic treatment is of particular importance when one is concerned

[1] This chapter is based on a previously published paper – Tim Heaton-Burgess, Aron J. Cohen, Weitao Yang, and Ernest R. Davidson, J. Chem. Phys. 128, 114702 (2008)

with calculating excitation energies to Rydberg states within time-dependant DFT (TDDFT). Most of the popular exchange-correlation functionals in use suffer from an incorrect asymptotic decay, and as such can lead to errors in excess of 1eV for Rydberg transitions [99] if this issue is not appropriately addressed. Depending on the system under consideration, and on the information we wish to extract, both size extensitivity and a correct asymptomatic treatment of the exchange correlation potential may be important. It is this situation that we consider in the following.

4.2 The reference potential in the direct OEP procedure

The direct OEP approach of Yang and Wu [48, 80] constructs the KS potential in a finite basis, $\{g_t(\mathbf{r})\}$, as

$$v_s(\mathbf{r}) = v(\mathbf{r}) + v_0(\mathbf{r}) + \sum_t b_t g_t(\mathbf{r}), \tag{4.1}$$

where v is the external potential of the system under consideration and v_0 a fixed reference potential that will be the focus of this discussion. In this way the functional dependance of the energy upon the KS potential is transferred on to the coefficients $\{b_t\}$ and the problem of determining the ground state energy is formulated as an unconstrained minimization of the energy as a function of the $\{b_t\}$: $\min_{w(\mathbf{r})} E[\rho[w(\mathbf{r})]] = \min_{\{b_t\}} E(\{b_t\})$. The above construction for the KS potential yields the exchange-correlation potential at convergence as

$$v_{\mathrm{xc}}(\mathbf{r}) = v_0(\mathbf{r}) - v_J(\mathbf{r}) + \sum_t b_t g_t(\mathbf{r}). \tag{4.2}$$

The foremost purpose of the reference potential appearing in Eqs. 4.1 and 4.2 is to aid in the convergence of the basis set expansion by providing a reasonable approximation to the Kohn–Sham potential, while not explicitly contributing to the energy derivatives. The freedom associated with choosing v_0 can also be exploited so

to enforce the correct asymptotic behavior of the exact exchange-correlation potential upon an approximate v_{xc}. From Eq. 4.2, we see that for any basis set decaying more rapidly than $1/r$, the asymptotic behavior of the exchange-correlation potential generated by the direct OEP method will be determined by the combination $v_0 - v_J$. The exact exchange-correlation potential of a finite neutral system behaves asymptotically as $-1/r$ [100, 101, 102, 103] (and as $-1/r +$ constant on those sets of zero measure corresponding to any nodal surfaces of the HOMO [104, 105] – which we will not consider here), while the coulomb potential approaches N/r where N is the number of electrons. Therefore if we construct the reference potential to behave asymptotically as $(N-1)/r$ we will have imposed the correct asymptotic behavior upon the exchange-correlation potential derived from any approximate functional.

In their original presentation Yang and Wu choose v_0 to be the Fermi–Amaldi potential [81, 61] for a given fixed density distribution $\rho_0(\mathbf{r})$ (taken as the self consistent LDA density or, as we shall employ, the sum of Hartree–Fock atomic densities):

$$v_0(\mathbf{r}) = \frac{N-1}{N} \int \mathrm{d}\mathbf{r}' \; \frac{\rho_0(\mathbf{r}')}{|\mathbf{r} - \mathbf{r}'|}. \tag{4.3}$$

The asymptotic correction afforded by the Fermi–Amaldi potential within the direct OEP method has been analyzed in detail [104], showing expected improvement in HOMO and LUMO energies from uncorrected DFT. TDDFT excitation energies [88] have also shown corresponding improvements with this asymptotic correction.

Other forms for the reference potential have been studied, including a Yukawa form [106] and linear combinations of the Coulomb potential and the Slater–Dirac exchange potential [16]. The latter was used in conjunction with GGA and hybrid functionals where artificially enforcing the exact $-1/r$ asymptotic behavior with the Fermi–Amaldi potential can deteriorate the convergence achievable for transition metal complexes.

One criticism of using the Fermi–Amaldi form for the reference potential is that

the implementation based on it is intrinsically not size extensive. While the energy expression itself maintains size extensitivity, the explicit appearance of the number of electrons in the prefactor influence the OEP KS orbitals and the extent to which the basis set expansion can correct for this is not obvious.

To construct one possible reference potential satisfying both the asymptotic and size-extensivity conditions we consider the van Leeuwen-Baerends potential [60]. This model potential was inspired by the Becke88 exchange functional [107], where the asymptotic behavior of the exchange energy density was enforced by a studious choice for the form of the energy density. In this way, we construct a size-extensive reference potential which enforces the correct asymptotic behavior as

$$v_0^\sigma(\mathbf{r}) = \int \mathrm{d}\mathbf{r}' \, \frac{\rho_\sigma(\mathbf{r}')}{|\mathbf{r}-\mathbf{r}'|} - \beta\rho_\sigma^{1/3}(\mathbf{r}) \frac{x_\sigma^2(\mathbf{r})}{1+3\beta x_\sigma(\mathbf{r})\sinh^{-1}(x_\sigma(\mathbf{r}))}, \tag{4.4}$$

where $x_\sigma = |\nabla\rho_\sigma(\mathbf{r})|/\rho_\sigma^{4/3}(\mathbf{r})$ is the reduced density gradient and the density appearing within the potential will be taken as the sum of Hartree–Fock atomic densities. While this potential has a variable parameter β, we could treat this as an additional variational degree of freedom in the OEP minimization by introducing the derivative

$$\frac{\partial E}{\partial \beta} = \int \mathrm{d}\mathbf{r} \, \frac{\delta E}{\delta v_s(\mathbf{r})} \frac{\partial v_0(\mathbf{r})}{\partial \beta}. \tag{4.5}$$

In practise we observe very little variation of the potential and energy with β and as such will use $\beta = 0.05$ [60].

In addition to the Fermi–Amaldi and van Leeuwen-Baerends forms, we will also consider as a reference potential the Coulomb potential associated with the sum of Hartree–Fock atomic densities. In this situation, the OEP calculation will be analogous to the conventional DFT approach and the inherent asymptotic behavior of whichever exchange-correlation functional we use will be manifested. Trivially this form will ensure our calculations are size extensive.

Size extensivity and correct asymptotics can also be achieved in other approaches to the OEP problem. For the matrix formulation of the OEP integral equation this can be achieved with a appropriate selection of basis functions for expanding the exchange-correlation potential [74, 94]. A correct asymptotic treatment can be obtained even on HOMO nodal surfaces with the method of Kümmel and Perdew [108]. In this approach the OEP can be constructed by iterating the potential with the function $S(\mathbf{r}) = \sum_{i=1}^{N} \psi_i^*(\mathbf{r})\phi_i(\mathbf{r}) + \text{c.c.} = \delta E/\delta v_s(\mathbf{r})$. This is, however, simply the the steepest decent direction of the energy functional written in terms of the orbital shifts ψ_i and KS orbitals $\phi_i(\mathbf{r})$. In this way we see the formal equivalence between the Yang–Wu direct minimization method and the Kümmel–Perdew indirect implementation of a steepest decent minimization in the potential variable.

4.3 Results

All calculations were performed within a locally modified version of NWChem [90] using Cartesian Gaussian basis sets. Thus the results associated with the Dunning basis sets [92, 109] in the following tables and figures are different from the conventional results associated with these basis sets using spherical harmonics. Energies are converged to at least 10^{-10} E_h with corresponding OEP energy gradients, $||\partial E^\text{OEP}/\partial \mathbf{b}||_1$, typically no greater than 10^{-6}. A singular value decomposition cutoff of 10^{-8} is used with the approximate Hessian associated with Newton minimization of the OEP energy. This value, together with inherently balanced basis sets, ensures a meaningful solution for the OEP [110] unless otherwise stated.

The size extensivity error (SEE) for a given reference potential is calculated as $\text{SEE}(M) = ME(M = 1) - E(M)$, where $E(M)$ is the ground state energy of a supermolecule comprised of M monomers (we restrict our presentation to $1 \leq M \leq 6$, however calculations have been performed up to $M = 20$ in some cases) separated by 20000 Å from one another in a linear cluster and $E(M = 1)$ is the

single monomer energy. We will consider clusters comprised of HF, N_2, and F_2 molecules with monomer bond lengths of 0.917Å, 1.098Å, and 1.417Å respectively.

We first examine the size extensivity of the direct OEP implementation when using the Fermi–Amaldi reference potential.

Figs. 4.1 and 4.2 show the EXX OEP size extensivity error as a function of the number of monomers in N_2 and HF supermolecule clusters respectively. Coinciding orbital and potential basis sets are used in these calculations as this balanced choice of basis sets allows for routine implementation without the generation of nonphysical potentials. Of course for linear molecules, only basis functions of Σ symmetry actually contribute to the expansion of the potential.

The SEE is seen to follow a near linear behavior as a function of the number

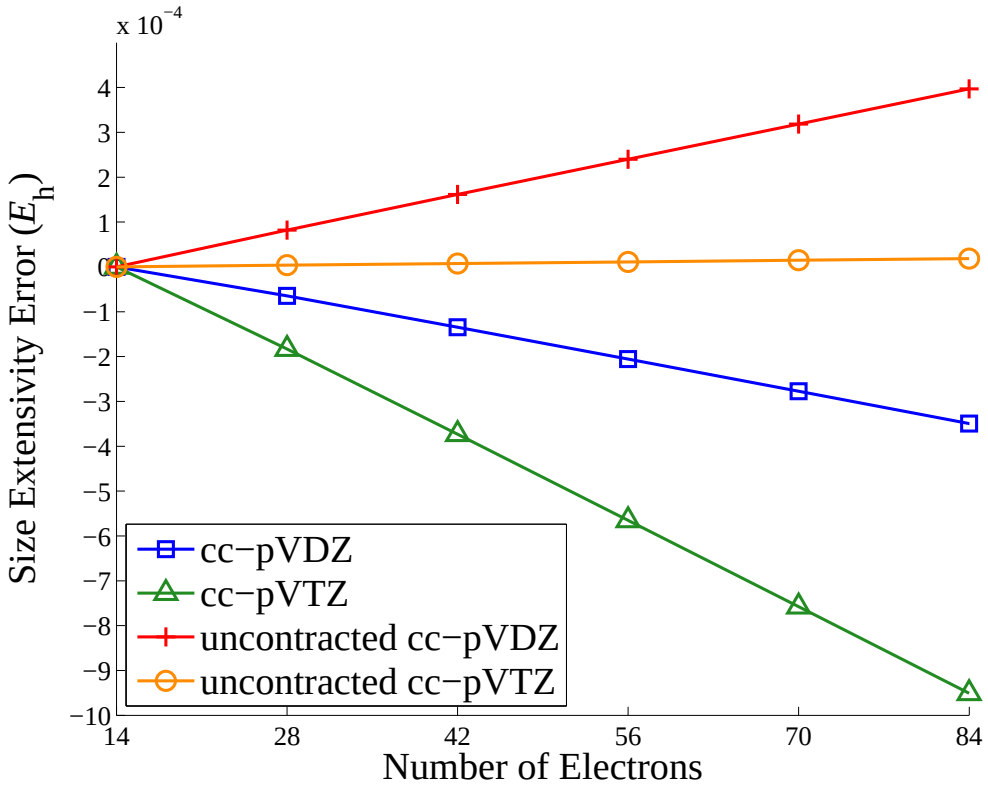

FIGURE 4.1: Exact-exchange OEP size extensitivity error as a function of the number of N_2 molecules when employing the Fermi–Amaldi reference potential. Coinciding orbital and potential basis sets are used.

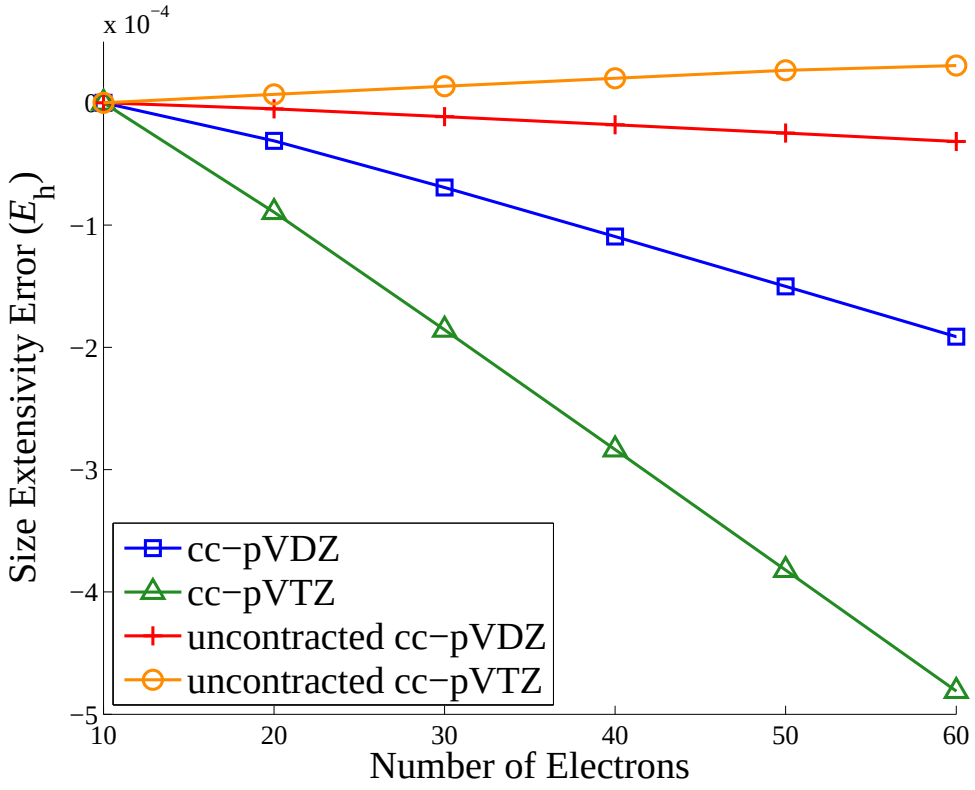

FIGURE 4.2: Exact-exchange OEP size extensitivity error as a function of the number of HF molecules when employing the Fermi–Amaldi reference potential. Coinciding orbital and potential basis sets are used.

of monomers (and continues to do so for $M > 6$) with the adherence to linearity becoming stronger as M increases. To understand this behavior we consider the SEE in the limit of an infinite number of monomers. As $N \to \infty$, the Fermi–Amaldi potential with its $(N-1)/N$ prefactor approaches the Coulomb potential. As such, the OEP energy obtained by using the Fermi–Amaldi and Coulomb reference potentials will coincide in this limit. Employing the exact size extensivity of the energy obtained when using a Coulomb reference potential (that is, $E^{\mathrm{Coulomb}}(M) = ME^{\mathrm{Coulomb}}(1)$) we can therefore write the limiting form of the SEE as

$$\mathrm{SEE}(M \to \infty) = M\Delta\widetilde{E} \tag{4.6}$$

where $\Delta\widetilde{E} = E^{\mathrm{FA}}(M=1) - E^{\mathrm{Coulomb}}(M=1)$ is the energy difference of two OEP

Table 4.1: SEE(M) − SEE($M-1$) in hartrees, where M is the number of HF monomers, calculated with three different basis sets (all employing the Fermi–Amaldi reference potential). The final row, denoted as $M=\infty$, corresponds to the asymptotic value $\Delta\tilde{E}$ of Eq. 4.6 calculated as $E^{\mathrm{FA}}(M=1) - E^{\mathrm{Coulomb}}(M=1)$.

M	3-21G	cc-pVDZ	uncontracted cc-pVDZ
2	4.063×10^{-4}	-3.112×10^{-5}	-5.061×10^{-6}
4	3.802×10^{-4}	-4.003×10^{-5}	-6.643×10^{-6}
6	3.772×10^{-4}	-4.112×10^{-5}	-6.834×10^{-6}
10	3.758×10^{-4}	-4.160×10^{-5}	-6.912×10^{-6}
∞	3.751×10^{-4}	-4.184×10^{-5}	-6.926×10^{-6}

calculations performed on a single monomer utilizing the Fermi–Amaldi and Coulomb reference potentials. This is a pleasing result in as much as we expect the value of $\Delta\widetilde{E}$ to be small – the Fermi–Amaldi potential modifies the uncorrected KS potential mainly in the long range part which has been seen to have a small effect upon on the total energy [104] relative to the uncorrected potential. What we can not easily deduce formally is how the SEE behaves for small M and in particular the manner in which the large M linear behavior is approached. Figs. 4.1 and 4.2 interestingly show that this limiting form is in fact reached very rapidly. Table 4.1 presents numerical values for the SEE slope as a function of the number of HF monomers for three different basis sets, together with a direct calculation of the limiting value $\Delta\tilde{E}$ as defined by Eq. 4.6. We see that even for two monomers the slope is within a factor of 1.5 for the limiting value in all three cases. Table 4.1 also displays how small $\Delta\tilde{E}$ can be. For the smallest, least flexible, basis set it obtains the value $3.8 \times 10^{-4} E_{\mathrm{h}}$, which decreases to $6.9 \times 10^{-6} E_{\mathrm{h}}$ for the largest basis set.

Another significant observation is that the magnitude of the SEE is rather small for these combinations of orbital and potential basis sets – even for the largest clusters we consider the error is smaller than 1 kcal mol^{-1}. The magnitude of the SEE is seen to be dependant upon the size of the potential basis set. Decontracting basis sets generally result in a substantial decrease of the SEE, especially as larger basis sets

Table 4.2: The size extensivity error in hartrees for HF and F_2 dimers calculated with various basis sets. Coinciding orbital and potential basis sets are used.

Basis Set	HF	F_2
6-31G	4.80×10^{-4}	1.27×10^{-3}
6-311G	3.13×10^{-4}	3.32×10^{-4}
6-31++G	6.37×10^{-4}	9.18×10^{-4}
6-311++G**	1.11×10^{-5}	-6.61×10^{-5}
cc-pVDZ	-3.11×10^{-5}	8.35×10^{-4}
cc-pVTZ	-8.95×10^{-5}	-1.98×10^{-5}
aug-cc-pVDZ	-1.04×10^{-4}	4.88×10^{-5}
aug-cc-pVTZ	2.91×10^{-5}	-2.24×10^{-5}

are considered. This is understandable as the lack of size extensitivity arises from the potential used to construct the Kohn–Sham orbitals, rather than an inherently non-size extensive energy functional. Table 4.2 displays the SEE for two F_2 molecules for a range of basis sets. We see that the smallest basis sets give a more significant error – for the 6-31G basis set the 1 kcal mol^{-1} mark is almost reached. While these basis sets are trivially too small for the fluorine molecule, OEP calculations of larger molecules have employed such basis sets and as such the SEE will be significant in these calculations when using the Fermi–Amaldi reference potential. One can imagine the calculation of charge transfer and excitations in large, spatially separated molecules, would be affected to some significant degree, as would potential curves for fragmentation of clusters and dissociation energies calculated using supermolecule limits.

To illustrate the significant effect of the potential basis set consider Fig. 4.3 in which we keep the orbital basis fixed as cc-pVTZ and calculate the EXX OEP SEE for the progression of potential basis sets cc-pV(D,T,Q,5)Z. For a single HF molecule, the number of independent symmetry-allowed potential basis functions are 10, 20, 36, and 60 for the double- through quintuple-zeta basis sets. Both double- and triple-zeta basis sets are insufficient to provide an adequate representation of the exchange

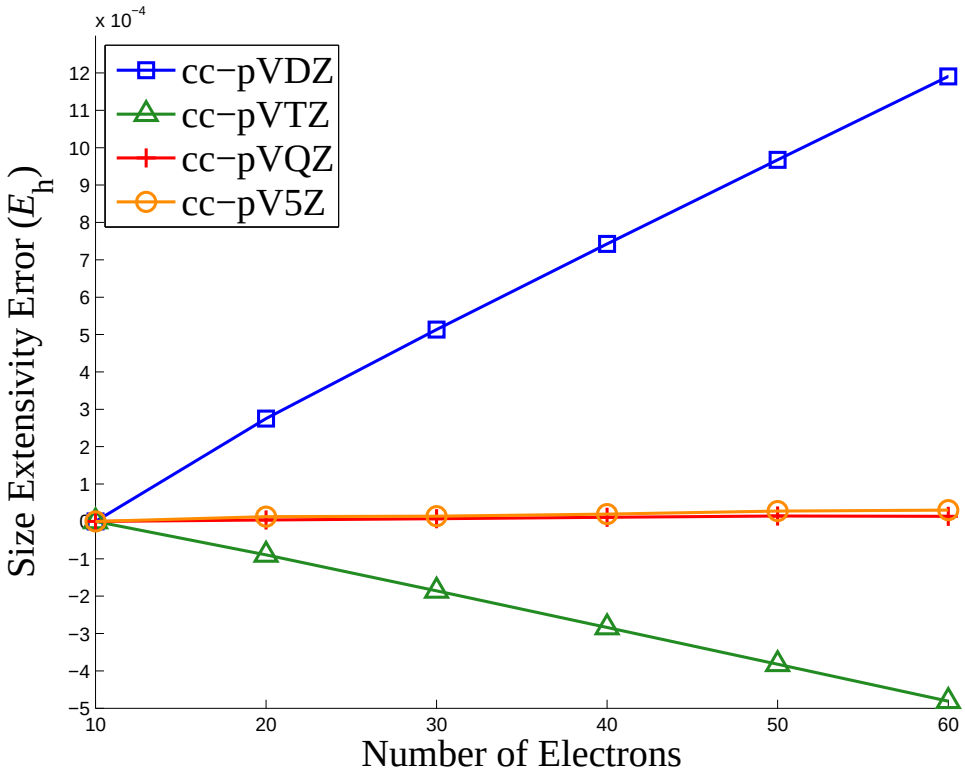

FIGURE 4.3: Effect of the potential basis set upon the size extensivity error. The orbital basis set for all calculations is cc-pVTZ and the potential basis set is varied as indicated. For double- through quintuple-zeta potential basis sets, the size extensivity error for M=2 are 2.8×10^{-4}, -9.0×10^{-5}, 3.7×10^{-6}, and 1.3×10^{-5} E_h respectively.

potential for this molecule. The double zeta potential basis calculation yields a featureless exchange potential, as too does the TZ potential basis which also suffers from poor asymptotic behavior. The QZ potential basis captures the finer details of the HF potential, while the 5Z basis suffers from extensive nonphysical oscillations (and would require an L-curve analysis to extract a physical potential [110]). The QZ and 5Z potential basis sets yield significantly smaller SEE's than the DZ and TZ basis sets as we would expect based on dimensionality and flexibility arguments.

The effect of the exchange-correlation energy functional employed in the OEP calculation for a HF supermolecule with the cc-pVTZ orbital and potential basis is

shown in Fig. 4.4. Four popular functionals including LDA (SVWN5), a GGA and two and hybrids (all of which have an incorrect asymptotic decay), in addition to EXX are shown. Such asymptotically-corrected calculations with these functionals that do not necessarily warrant an OEP approach are useful when one considers TDDFT Rydberg excitation energies [99] which require an asymptotic correction scheme for accurate results. We see that all exchange-correlation functionals used rapidly approach the limiting linear behavior and maintain the small magnitude we have observed with the EXX functional.

We finally consider some calculations employing the reference potential of Eq. 4.4. Table 4.3 displays the total exact-exchange energies and size-extensivity errors

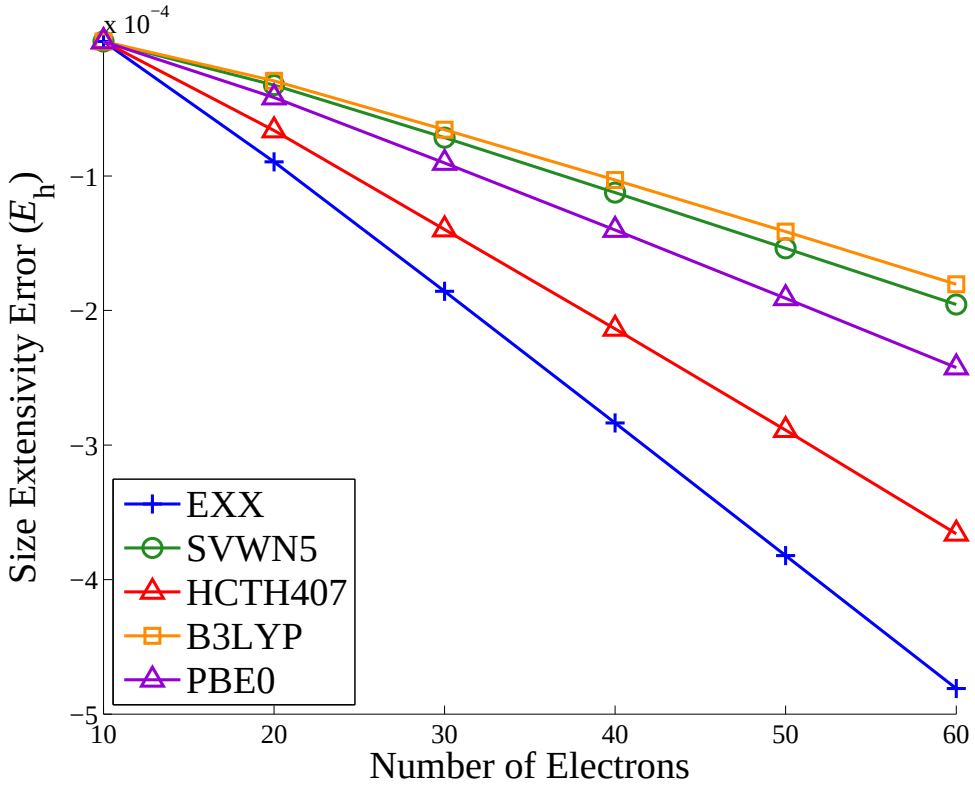

FIGURE 4.4: Size extensivity error for HF with various exchange-correlation functionals implemented within the OEP approach employing the Fermi–Amaldi reference potential. The orbital and potential basis set is cc-pVTZ for all functionals.

Table 4.3: Exact-exchange OEP energies and size-extensivity errors (both in hartrees) for two HF molecules with various reference potentials. FA refers to the Fermi–Amaldi potential, and LB to Eq. 4.4. Coinciding orbital and potential basis sets are used.

Basis Set	Method		E(HF)	E(2HF)	|SEE|
cc-pVTZ	HF		-100.058 877	-200.117 754	0.000 000
	OEP	FA	-100.057 952	-200.115 813	0.000 092
		Coulomb	-100.057 851	-200.115 702	0.000 000
		LB	-100.057 878	-200.115 756	0.000 000
uncontracted-cc-pVTZ	HF		-100.058 937	-200.117 875	0.000 000
	OEP	FA	-100.056 991	-200.113 988	0.000 007
		Coulomb	-100.056 997	-200.113 994	0.000 000
		LB	-100.057 004	-200.114 009	0.000 000
aug-cc-pVDZ	HF		-100.034 785	-200.069 569	0.000 000
	OEP	FA	-100.033 659	-200.067 215	0.000 102
		Coulomb	-100.033 555	-200.067 111	0.000 000
		LB	-100.033 763	-200.067 526	0.000 000
aug-cc-pVQZ	HF		-100.069 448	-200.138 895	0.000 000
	OEP	FA	-100.067 934	-200.135 870	0.000 001
		Coulomb	-100.067 938	-200.135 876	0.000 000
		LB	-100.067 979	-200.135 958	0.000 000

calculated for two HF molecules with the Fermi–Amaldi (FA), Coulomb, and van-Leeuwen–Baerends (LB) reference potentials for the aug-cc-pVDZ and aug-cc-pVQZ basis sets. The van-Leeuwen–Baerends potential provides a slightly lower energy than the Fermi–Amaldi potential and is exactly size-extensive. The Coulomb potential is also size-extensive, however does not provide the asymptotic correction we often desire. One other simple possibility to ensure size-extensitivity is to use no reference potential at all, although this is more susceptible to the generation of nonphysical potentials and convergence issues occasionally arise.

Fig. 4.5 shows the OEP's for a neon atom generated by using LDA (SVWN5) as the exchange-correlation functional and employing the Coulomb, Fermi–Amaldi and van Leeuwen–Baerends reference potentials. While an OEP approach is not

required for the LDA functional, this provides a clear example of the effect of the reference potential upon correcting the inherently incorrect asymptotic behavior of an approximate exchange-correlation potential (in this case, the LDA potential is exponentially decaying). The Fermi–Amaldi and van Leeuwen–Baerends reference potential provide asymptotically corrected LDA potentials, however at the expense of losing size-extensitivity in the case of the Fermi–Amaldi potential. The uncorrected LDA OEP generated with the Coulomb reference potential displays the intrinsic exponential decay of the LDA functional and agrees well (although the agreement

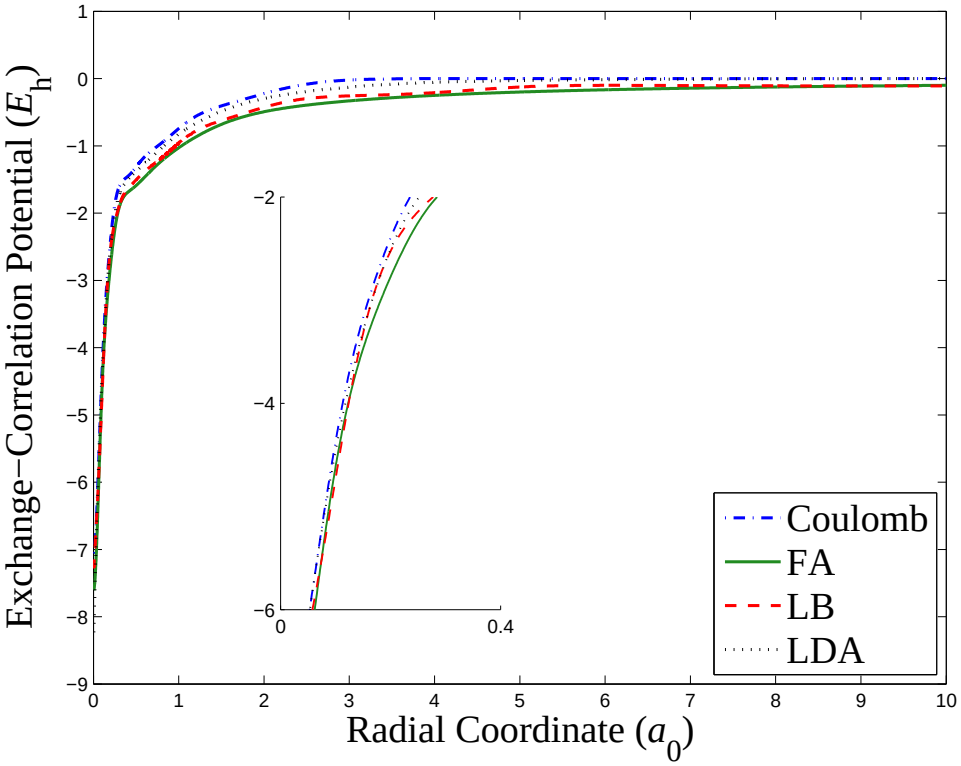

FIGURE 4.5: LDA (SVWN5) potentials of neon calculated within the OEP approach for the reference potentials considered in this chapter. The atomic basis set is aug-cc-pVTZ (6d/10f) and the potential basis set consists of 9 s-type Gaussian functions with exponents $2^n, n = -1, 0, \cdots, 7$. Also included is the LDA potential obtained from a conventional DFT calculation, which closely resembles the LDA OEP generated with a Coulomb reference potential. The Fermi–Amaldi and van-Leeuwen–Baerends reference potentials give rise to the slower $-1/r$ decay.

Table 4.4: Comparison of OEP (employing the LDA functional) energies (in hartrees) of the neon atom for the three reference potentials considered within this chapter. Basis sets are those of Fig. 4.5. For comparison, the final column displays the energies from a conventional DFT calculation employing the LDA functional. The experimental ionization energy is 0.792 E_{h}.

	Coulomb	Fermi–Amaldi	LB	DFT
E^{LDA}	-128.220 452 5	-128.220 461 4	-128.220 460 1	-128.220 461 7
1s	-30.1995	-30.5063	-30.4400	-30.3101
2s	-1.2399	-1.5209	-1.4517	-1.3246
2p	-0.4126	-0.6947	-0.6247	-0.4982
3s	0.1687	-0.1072	-0.4152	0.0891
3p	0.2188	-0.0364	0.2635	0.1539
4s	0.9104	0.6466	0.7102	0.8393
3d	0.9794	0.6948	0.7661	0.8915

is limited by the chosen potential basis set) with the exact LDA potential. Both Fermi–Amaldi and van-Leeuwen–Baerends reference potentials correct this, however it is seen the decay of the van-Leeuwen–Baerends potential is faster than that of the Fermi–Amaldi. This could not be corrected by varying β. The faster decay of the potential is manifested in the orbital energies of Table 4.4 where it is seen the HOMO energy when using the van-Leeuwen–Baerends potential is improved (relative to the experimental ionization energy of 0.792 E_{h}) from the uncorrected value, however is 0.07 E_{h} smaller than the corresponding value when employing the Fermi–Amaldi potential. Both of these forms support a Rydberg series in the complete basis set limit whereas the exponentially decaying potentials from the Coulomb reference potential calculation do not.

4.4 Conclusion

We have studied the size-extensitivity of the direct OEP method of Yang and Wu when the Fermi–Amaldi potential is employed as the reference potential for the construction of the Kohn–Sham potential. The size-extensitivity error rapidly approaches a limiting linear form in the number of monomers while maintaining a

relatively small magnitude for all but the smallest of basis sets. For reasonably flexible potential basis sets, the error is rather small and can be essentially ignored given a large enough basis set. Considering that the computational expense of the direct OEP method is not much more than a conventional DFT calculation, there is little reason why one should restrict calculations to small potential basis sets and as such the size-extensitivity error we observe should not warrant a major consideration for small to moderately sized systems. These observations hold for all the exchange-correlation functionals we have examined.

We also considered one possible reference potential that is size-extensive and also provides an asymptotic correction for approximate exchange-correlation potentials.

For exchange-correlation functionals depending explicitly upon the KS orbitals or eigenvalues, OEP approaches are the only way to correctly perform Kohn–Sham density functional calculations. The Yang–Wu direct approach provides a computationally accessible OEP implementation for large molecules where an understanding of the methods size-extensitivity is essential.

5

A Manifestation of the Delocalization Error of Density Functional Approximations: Structures of C_{4N+2} Rings

5.1 Introduction

In this last chapter we will move away from the potential-based aspects so far considered and study a particular system where common density functionals fail quite dramatically – predicting the structures of C_{4N+2} rings. Rather than being a computational study intended to elucidate various properties of this system, we are more concerned about the functionals themselves – when and why they fail. Several of the functionals we employ here are implicit density functionals but we do not invoke the OEP procedure to evaluate them. We can get away with this as they depend only upon occupied Kohn–Sham orbitals, and because the reason why they fail is related to only one issue – the delocalization error – which can be adequately addressed in this system with such functionals.

The ground state structure of C_{4N+2} rings are believed exhibit a geometric transition from angle-alternation ($N \leq 2$) to bond-alternation ($N > 2$). All previous

density functional theory (DFT) studies on these molecules have failed to reproduce this behavior by predicting either that the transition occurs at too large a ring size, or that the transition leads to a higher symmetry cumulene. Employing the recently proposed perspective of delocalization error within DFT we will rationalize this failure of common density functional approximations (DFAs) and present calculations with the rCAM-B3LYP exchange-correlation functional that correctly predicts the structural evolution of this system. The behavior exemplified here manifests itself more generally as the well known tendency of DFAs to bias towards delocalized electron distributions as favored by Hückel aromaticity, of which the C_{4N+2} rings provide a quintessential example. An unbiased treatment of delocalization is one of many stabilization mechanisms that must be appropriately treated in more complex molecules. The relative energies of the C_{20} ball, cage, and ring isomers are such examples.

5.2 Background

Density functional theory is a popular approach for modeling large carbon-based systems where competing effects such as Hückel aromaticity, electron correlations, and symmetry breaking are significant and must be approached with rigor while maintaining computationally feasibility. With linear scaling approaches being well developed the opportunity to investigate ever more complex systems with DFT is an attractive prospect. Yet, there are many situations where density functional approximations (DFA) to the exchange-correlation functional of DFT can generate unacceptable errors.

One well known issue of DFT that is of particular importance to large carbon structures is the tendency of the popular DFAs to bias towards homogenized electron distributions. This observation has long been noted in small molecules where DFAs often overbind systems where delocalized electron distributions are a possibility [23].

Such biasing can significantly distort molecular geometries as has been seen clearly in oligomers, where bond length alternation is suppressed by all common forms of non-long-range corrected DFAs [111, 112]. In it most extreme form this failure of DFAs can completely negate stabilizing mechanisms giving rise to incorrect molecular geometries as will be shown here with C_{4N+2} rings.

Three ground state structures are considered for these rings: a high symmetry cumulene ($D_{(4N+2)h}$ – all bong lengths and bond angles are equal) together with two reduced symmetry ($D_{(2N+1)h}$) forms – an angle-alternating cumulene and a bond length-alternating (acetylenic) structure. These structures provide a sensitive test for the unbiased treatment of delocalization by DFAs owing to the presence of a second-order Jahn–Teller effect stabilizing the reduced symmetry forms relative to the high symmetry cumulene. So far, DFAs have been unable to correctly describe the structural evolution of this system. We will show that this failure of existing exchange-correlating functionals can be avoided with a correct understanding of the delocalization properties of DFAs. As such, this marks the first application of DFAs designed to minimize delocalization errors to this system which has had a history of conflicting results when comparing density functional based calculations with different functionals and wave function methods [113, 114, 115, 116, 117, 118]. The behavior we observe here, and more importantly the fundamental understanding that has been recently provided which allows us to correctly deal with these systems, will be essential for the future development of exchange-correlation functionals suitable for dealing with large carbon structures where many stabilizing mechanisms compete directly with Hückel aromaticity. We will also present calculations on the bowl, cage and ring isomers of C_{20}, another system with a confusing history [119, 120, 121], where the presence of a delocalization error may effect the energetic ordering.

Many of the systematic failures of DFAs are due to the delocalization error (DE) [26, 21]. These include the overestimation of oligomer polarizabilities [122] and the

underestimation of band gaps [25] and reaction barriers [123]. The DE is the incorrect behavior of the ground state energy as a function of the number of electrons. The exact many-body ground state energy is a piecewise linear function interpolating the energy at integral numbers of electrons [124, 125]. Deviation from this straight line behavior represents an error – a convex curve for the total energy, as is typical of most density functionals, stabilizes the energy at non-integer numbers of electrons and is termed the DE. Conversely, a concave curve, as obtained from Hartree–Fock (HF) theory, represents a localization error. The DE is most naturally observed in the fragmentation of molecules to infinite separation, where it leads to too low energy with electrons delocalized over different fragments. The relationship between delocalization and localization errors in stabilizing delocalized/localized density distributions at near-equilibrium geometries is less transparent. Perhaps the most prominent structural effects correlated with DE is the bond length alternation (BLA) observed in oligomers [111], where the alternation predicted by common DFAs is too small (the electron distribution is too delocalized), and decays too rapidly with the oligomer length, compared to wave function theories. Long-range corrected functionals such as CAM-B3LYP and LC-PBE have been shown to significantly improve the description of BLA relative to hybrids, GGAs and LDA [112, 126]. This trend follows that of the delocalization error typically seen in each class of functional [24].

The highest level of calculations that have been performed on the C_{4N+2} system are the quantum Monte Carlo (QMC) and limited coupled cluster (CCSD) calculations of Torelli and Mitas [113]. These calculations predicted a crossover from angle- to bond-alternating structures between C_{10} and C_{14}, with the higher symmetry cumulene present as a transition state. It should be noted that the structures employed by Torelli and Mitas are approximations to the local minima as they were obtained by a sampling forces under bond length variations rather than a full geometry optimization.

Hartree–Fock calculations show the same transition as QMC, albeit significantly overestimating the relative stability of the bond alternating form, which can be rationalized as a manifestation of the localization error of HF. DFT calculations on this system have yielded strongly functional-dependant results, all of which conflict with the QMC and HF results. LDA and GGA functionals show a transition from angle-alternation to the higher symmetry cumulene between C_{10} and C_{14}. These functionals have the largest delocalization error resulting in an overstabilization of the aromatic structure to the extent of completely negating the second order Jahn–Teller effect. Only extrapolating to the infinite limit has given rise to a stable bond-alternating structure as induced by a Peierls mechanism [127]. The B3LYP hybrid functional improves upon this result [115, 116], giving rise to the correct transition from angle- to bond-alternation but this occurs between C_{18} and C_{22} (or between C_{22} and C_{26} [117]). The inclusion of Hartree–Fock exchange decreases the delocalization error and we see this manifested in the better performance of B3LYP. A recent CCSD study by Arulmozhirajaa and Ohno [118] predicted a structure with both bond and angle alternation to be the most stable form for C_{14}, C_{18}, and C_{22}, and the bond-alternating structure to be more stable than the angle-alternating cumulene. We will comment on this result below.

Only recently have exchange-correlation functionals been explicitly designed in an attempt to minimize the delocalization error. Two functionals, MCY3 and rCAM-B3LYP, attempt to do so by including a fit to the straight line behavior of the total energy for the ionization and electron capture of a carbon atom when constructing the functionals [24]. Here we employ rCAM-B3LYP, a reparametrization of CAM-B3LYP [128], implemented within a modified version of the Dalton code [129] to perform geometry optimizations on C_{4N+2} rings, with the 6-311G* basis set. Calculations with the CAM-B3LYP, B3LYP, PBE0, PBE, BLYP, and LDA (SVWN5) functionals, and with Hartree–Fock theory, were also performed.

Table 5.1: Ring size at which the angle-alternating structure transitions to the bond-alternating (BA), aromatic (AR), or bond- and angle-alternating (B&AA) form for various exchange-correlation functionals.

Functional	Transition
rCAM-B3LYP	$C_{10} \rightarrow C_{14}$ (BA)
CAM-B3LYP	$C_{10} \rightarrow C_{14}$ (B&AA)
B3LYP, PBE0	$C_{18} \rightarrow C_{22}$ (BA)
BLYP, PBE, LDA	$C_{10} \rightarrow C_{14}$ (AR)
QMC[113]	$C_{10} \rightarrow C_{14}$ (BA)

5.3 Results

5.3.1 C_{4N+2} rings

Fig. 5.1 displays the energies of the angle- and bond-alternating structures relative to the aromatic form calculated with the rCAM-B3LYP and B3LYP functionals, and within HF and CCSD [118] theory. For clarity we exclude those functionals from Fig. 5.1 for which the bond-alternating structure is not stable for small rings (LDA, BLYP, and PBE), and the CAM-B3LYP results. The observed behavior of all the functionals studied is summarized in Table 5.1.

The rCAM-B3LYP functional predicts a transition from angle- to bond-alternation to occur between C_{10} and C_{14} in agreement with the QMC calculations of Torelli and Mitas [113]. This is the first density functional approximation to achieve this. The CAM-B3LYP functional, which was not designed with the delocalization error in mind but which displays a better fractional charge behavior than hybrid functionals, predicts the transition to occur between C_{14} and C_{18}, an improvement over B3LPY and PBE0 hybrids. While rCAM-B3LYP predicts the correct transition, the alternating structures are overly stabilized with respect to the QMC (by ~ 10 kcal/mol for C_{10} and C_{14}), although the improvement over HF is significant.

The CCSD results of Arulmozhirajaa and Ohno predict a bond- and angle-alternating structure to be most stable. We have been unable to converge to such

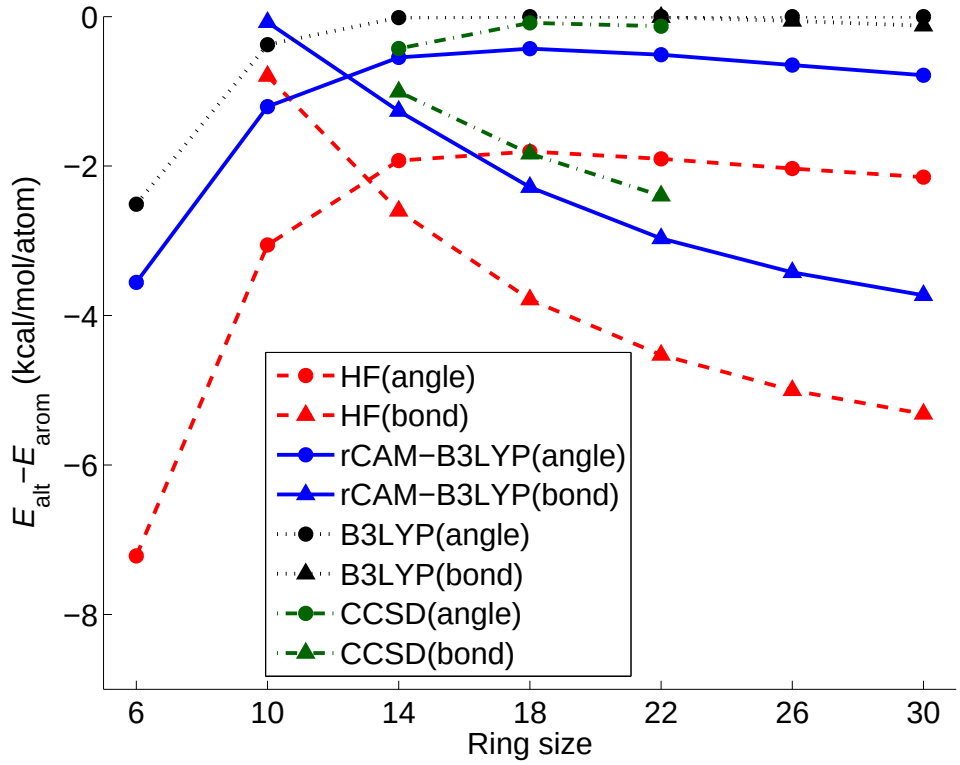

FIGURE 5.1: Energies of the bond- and angle-alternating structures relative to the aromatic ($D_{(4N+2)h}$) structure as a function of the ring size. rCAM-B3LYP gives rise to the structural transition between C_{10} and C_{14}. The CCSD values are taken from Arulmozhirajaa and Ohno (employing the 6-31G* basis set).

a structure with rCAM-B3LYP and the 6-311G* basis set. However, when using 6-31G*, D95(d,p) or cc-pVDZ basis sets that Arulmozhirajaa and Ohno employed, we do observe this structure to be the lowest in energy indicating some basis set effects with our DFT approach. Test calculations employing larger basis sets also failed to converge to such a structure. Further investigation is required to see if this effect is also present with CCSD, and also to understand the CAM-B3LYP results. Comparing rCAM-B3LYP relative energies (ignoring the bond- and angle-alternating structure) to these CCSD results we see a much better agreement than with QMC. With the 6-31G* basis set, CCSD predicts the C_{14} acetylenic and cumulenic forms to lie 14.05 kcal/mol and 5.98 kcal/mol below the aromatic structure respectively,

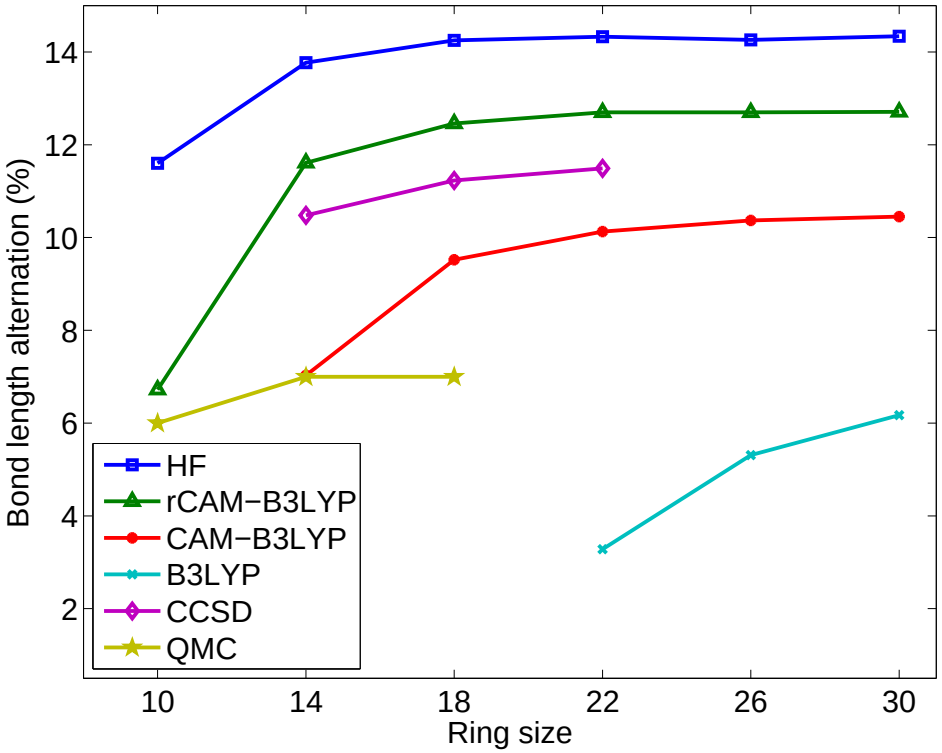

FIGURE 5.2: Bond length alternation as a function of ring size. The CCSD results are from Arulmozhirajaa and Ohno (employing the 6-31G* basis set) and QMC from Torelli and Mitas.

with rCAM-B3LYP yielding 17.64 kcal/mol and 7.56 kcal/mol. The bond length alternation (BLA) – the difference in bond lenghts divided by the mean bond length – is shown in Fig. 5.2 for various functionals and the CCSD and QMC results discussed above. For C_{14} rCAM-B3LYP and HF predict the BLA to be 1.13% and 3.29% higher than CCSD respectively, while the values used in Torelli and Mitas's QMC study are 4.61% lower. That the QMC structures are only approximate minima likely contributes to this large difference but it is unclear to what extent. The behavior of rCAM-B3LYP, B3LYP, LDA and HF for fractional numbers of electrons is exemplified in Fig. 5.3 for C_{14}. The maximum pointwise deviation from straight line behavior is 3.7 kcal/mol for rCAM-B3LYP, 5.7 kcal/mol for HF, 9.3 kcal/mol for B3LYP, and 12.4 kcal/mol for LDA. The rCAM-B3LYP deviation is similar to what

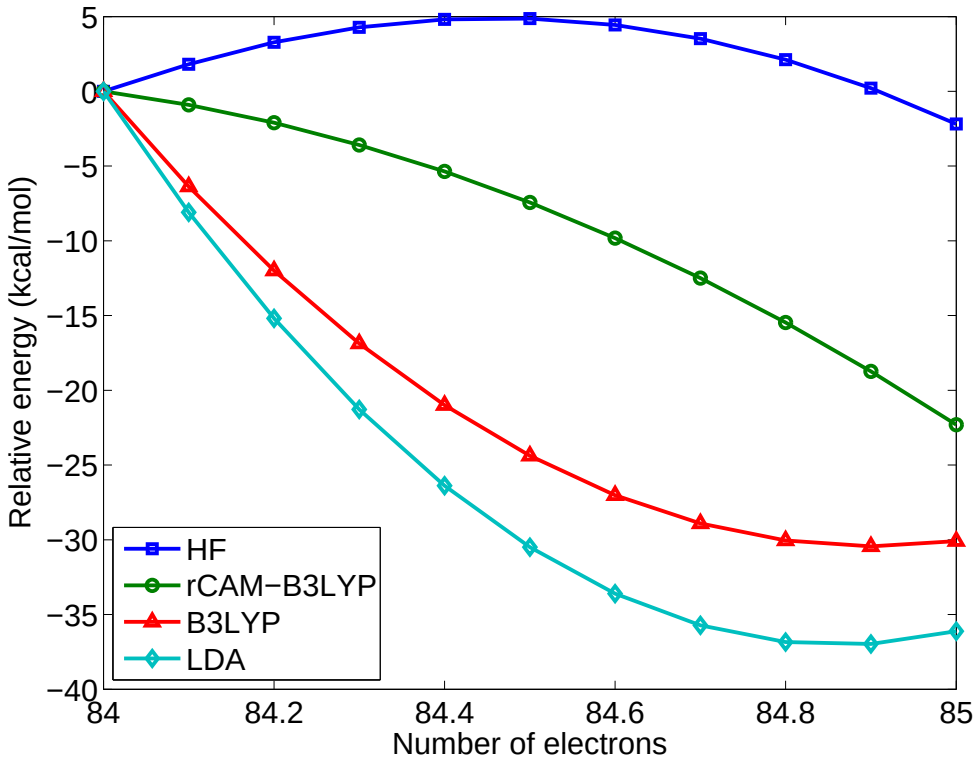

FIGURE 5.3: Relative energy of C_{14} (most stable structure of each functional) with fractional numbers of electrons.

was observed in an investigation of the energetics of Diels-Alder reactions [123].

Another manifestation of the delocalization error of DFAs is an incorrect treatment of the HOMO–LUMO gap [25]. Fig. 5.4 shows the gap for the lowest energy structures as a function of the ring size for various functionals. For this system we do not have high level results to compare with but we can understand the trend and observe that the rCAM-B3LYP results improve upon other functionals. LDAs and GGAs greatly underestimate the gap as the convex curve for $E(N)$ underestimates the slope of E when approaching N from below, and overestimates from above. With HF, the slope from above is too small resulting in an overestimation of the gap. Hybrids improve upon GGAs as a result of their better $E(N)$ behavior from mixing with HF, with range-separated hybrids performing better than global

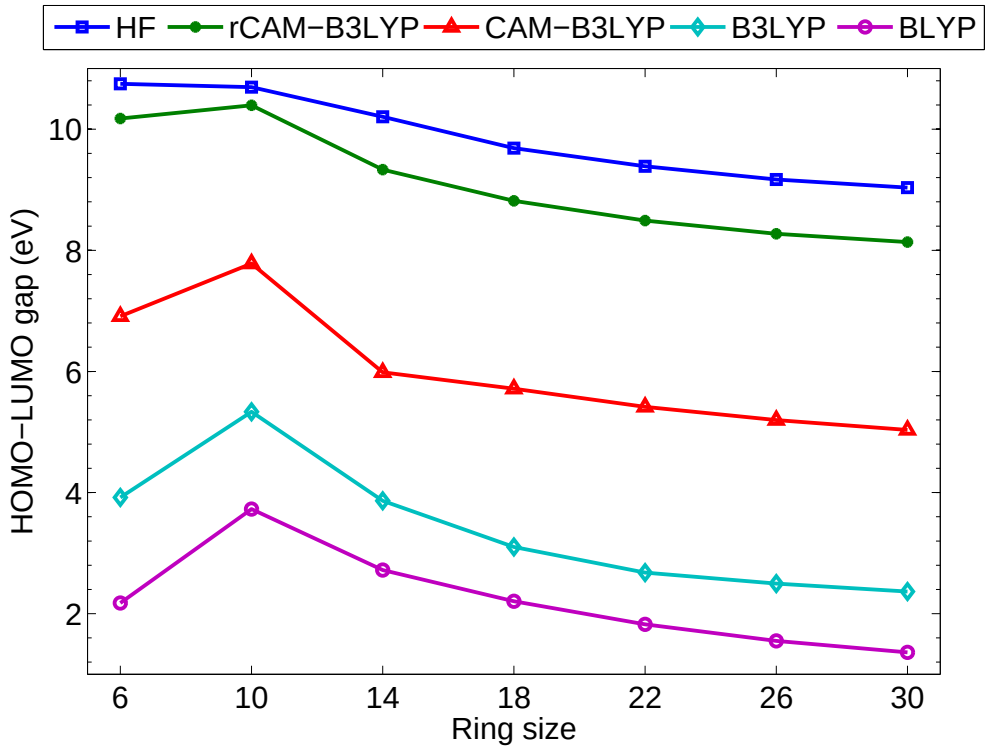

FIGURE 5.4: HOMO–LUMO energy gap for the most stable structure of each functional as a function of the ring size for several exchange-correlation functionals. Whilst not shown, the behavior of PBE0 is very similar to B3LYP; LDA (SVWN5) and PBE are very similar to BLYP.

hybrids [24]. From this argument we know that the correct value of the gap will fall between HF and CAM-B3LYP values, and this is what we see with rCAM-B3LYP. In the following section where consider isomers of C_{20} the HOMO–LUMO gaps we obtain with rCAM-B3LYP will be seen to be in very good agreement with coupled cluster calculations.

5.3.2 Ring, bowl, and cage isomers of C_{20}

We briefly consider one more system for which many conflicting DFT calculations exist – the ring, bowl, and cage isomers of C_{20}. The relative energies and the HOMO–LUMO gap of the isomers are shown in Tables 5.2 and 5.3. Both rCAM-B3LYP and

Table 5.2: Relative energies (eV) of the bowl, cage, and ring isomers of C_{20}.

Method	Bowl	Cage	Ring
CAM-B3LYP/cc-pVDZ	**0.0**	0.86	1.11
rCAM-B3LYP/cc-pVDZ	**0.0**	0.66	2.09
CCSD(T)/cc-pVDZ//PBE0/cc-pVTZ[130]	**0.0**	0.28	2.32
QMC[120]	**0.0**	2.15	1.06
B3LYP/cc-pVTZ[130]	0.0	1.89	**−0.90**

Table 5.3: HOMO–LUMO gap (eV) of the bowl, cage, and ring isomers of C_{20}.

Method	Bowl	Cage	Ring
CAM-B3LYP/cc-pVDZ	6.40	4.23	4.57
rCAM-B3LYP/cc-pVDZ	9.49	6.84	7.61
CCSD(T)/cc-pVDZ//PBE0/cc-pVTZ[130]	9.59	6.68	7.22
CCSD(T)/cc-pVDZ//MP2/cc-pVDZ[130]	9.13	6.38	6.52
B3LYP/cc-pVTZ[130]	3.72	1.93	2.07

CAM-B3LYP predict the same energy ordering, with the bowl isomer being the most stable and the ring the least. This ordering is in agreement with the CCSD(T) calculations of An *et al.* [130], where we also see reasonable agreement in the relative energies. Compared to their results, rCAM-B3LYP stabilizes the cage isomer by 0.38 eV and destabilizes the ring by 0.23 eV. The QMC results of Grossman *et al.* [120] also predict the bowl to be the most stable isomer, however the ordering of the cage and ring are swapped. We are unable to pinpoint the reason for this discrepancy. Hybrid functionals do not predict a consistent ordering of these isomers [130] indicting that the delocalization error is likely not the dominant source of error in determining the energy ordering. It is interesting to consider the HOMO–LUMO gap, for which the delocalization error is of utmost importance in any system as described previously for the C_{4N+2} rings. We obtain good agreement with CCSD(T) results – the rCAM-B3LYP results obtained directly from the HOMO and LUMO energies on the neutral species differ by 0.1 eV (bowl), 0.16 eV (cage), and 0.39 eV (ring) from CCSD(T)/cc-pVDZ//PBE0/cc-pVTZ calculations.

5.4 Conclusion

In summary, we have considered a structural manifestation of the delocalization error of density functional approximations. The C_{4N+2} rings provide a transparent picture of such effects on molecular structures owing to the presence of a second order Jahn–Teller effect competing with Hückel aromaticity to produce a range of structures representing both localized and delocalized densities. Employing the rCAM-B3LYP exchange-correlation functional, which was designed to have minimal delocalization error, we have correctly predicted the geometric transition between angle-alternation and bond-alternation between C_{10} and C_{14}. rCAM-B3LYP is one of the first functionals (along with MCY3) designed with the intent to minimize the delocalization error and the first to correctly describe this transition, emphasizing the importance of such functionals when studying systems where stabilizations mechanisms compete with Hückel aromaticity. Our results over-stabilize the structures with respect to QMC, however good agreement with CCSD is achieved. We have also applied the rCAM-B3LYP functional to the bowl, cage, and ring isomers of C_{20} where the delocalization error does not appear to be the dominant error. We obtained an energy ordering in agreement with CCSD but not with QMC. The HOMO–LUMO gaps we obtained agree well with CCSD calculations owing to the improved straight line behavior of the total energy.

6

Summary

This dissertation has examined some formal and computational aspects of the optimized effective potential approach, and addressed a manifestation of the delocalization error of density functional approximations.

In chapter 2 we have generalized the potential functional formalism of Yang, Ayers, and Wu to current-carrying systems in the presence of noncollinear magnetic fields. Here we provided a solution to two fundamental issues in such systems – the v-representability and nonuniqueness issues. The potential based approach readily lends itself to any particular Hamiltonian and could, for example, be further generalized to relativistic systems. We also suggested an implementation of the noncollinear OEP by direct minimization of the total energy with respect to the Kohn–Sham potentials in finite basis sets. While there are few functionals that yet require an OEP approach, some issues exist which would be of interest to examine with existing functionals. One aspect where hybrid functionals implemented via the OEP approach perform significantly better is with magnetic response properties of molecules. One wonders what differences would be observed when magnetic fields and currents are explicitly included. Also, tweaking the OEP implementation to invert densities so to

obtain the corresponding Kohn–Sham potentials, analogous to the Wu–Yang method in collinear systems, would allow for examination of the exchange-correlation vector potential in molecular systems. Further points of interest related to the potential-based approach that are yet to be examined include an analysis of the asymptotic behavior of the exchange-correlation magnetic and vector potentials, and an analysis of the potential–wavefunction nonuniqueness in relativistic systems.

Chapters 3 and 4 changed direction to focus on computational aspects of solving for the OEP in finite basis sets. To address the problem of generating nonphysical potentials when unbalanced orbital and potential basis sets are employed, we developed a robust regularization approach biasing towards smooth potentials and employing L-curve analysis to determine the optimal value of the regularization parameter. While the ideal approach to this problem would involve, for *any* given orbital basis set, being able to select *a priori* an exactly balanced potential basis set that is flexible enough to accurately describe the potential, it would seem unlikely that this is possible. Our regularization approach provides the next best solution – for any combination of unbalanced basis sets we find a meaningful solution. This method would easily be implemented within the approach suggested in chapter 2 for noncollinear systems. The size extensivity of the Yang-Wu OEP implementation was also analyzed and shown not to be a significant issue, particular when flexible basis sets are employed for the potential.

Finally, in chapter 5, we examined a manifestation of the delocalization error of density functional approximations in C_{4N+2} rings. We demonstrated that the delocalization error can negate stabilization mechanisms competing with Hückel aromaticity so to generate incorrect molecular geometries. In this example, a second order Jahn–Teller effect was negated, but the issue will be present where any form of symmetry breaking competes with Hückel aromaticity. By using a functional designed with the intent of addressing the delocalization error, we were able to obtain a geometric

transition in the ground state structure from angle-alternation and bond-alternation between C_{10} and C_{14}, in agreement with quantum Monte Carlo calculations. This is an example where orbital-dependant exchange-correlation functionals appear necessary to obtain correct results. Development of improved functionals to deal with the delocalization error and other issues, such as static correlation, are likely to include unoccupied orbitals which in turn necessitates an OEP approach for self-consistent implementation. The previous chapters, in particular chapter 3, have ensured that the OEP method employing such functionals will be able to be performed successfully.

Bibliography

[1] P. Hohenberg and W. Kohn. *Phys. Rev.*, 136:B864, 1964.

[2] M. Levy. *Proc. Natl. Acad. Sci. USA*, 76:6062, 1979.

[3] T. L. Gilbert. *Phys. Rev. B*, 12:2111, 1975.

[4] J. E. Harriman. *Phys. Rev. A*, 24:680, 1975.

[5] W. Yang, P. W. Ayers, and Q. Wu. *Phys. Rev. Lett.*, 92:146404, 2004.

[6] W. Kohn and L. J. Sham. *Phys. Rev.*, 140:A1133, 1965.

[7] V. L. Lignéres and E. A. Carter. An introduction to orbital-free density functional theory. In *Handbook of Materials Modeling*, chapter 1.8, pages 137–148. Springer Netherlands, 2005.

[8] P. A. M. Dirac. *Proc. Camb. Phil. Soc.*, 26:376, 1930.

[9] S. H. Vosko, L. Wilk, and M. Nusair. *Can. J. Phys.*, 58:1200, 1980.

[10] J. P. Perdew and Y. Wang. *Phys. Rev. B*, 33:8800, 1986.

[11] E. Engel and R. M. Dreizler. *J. Comp. Chem.*, 20:31, 1999.

[12] R. T. Sharp and G. K. Horton. *Phys. Rev.*, 90:317, 1953.

[13] J. D. Talman and W. F. Shadwick. *Phys. Rev. A*, 14:36, 1976.

[14] A. J. Cohen, Q. Wu, and W. Yang. *Chem. Phys. Lett.*, 399:84, 2004.

[15] O. B. Lutns, A. M. Teale, T. Helgaker, and D. J. Tozer. *J. Chem. Theory Comput.*, 2:827, 2006.

[16] A. M. Teale, A. J. Cohen, and D. J. Tozer. *J. Chem. Phys.*, 126:074101, 2007.

[17] J. B. Krieger, Y. Li, and G. J. Iafrate. *Phys. Rev. A*, 46:5453, 1992.

[18] O. V. Gritsenko and E. J. Baerends. *Phys. Rev. A*, 64:042506, 2001.

[19] F. Della Sala and A. Görling. *J. Chem. Phys.*, 115:5718, 2001.

[20] V. N. Staroverov, G. E. Scuseria, and E. R. Davidson. *J. Chem. Phys.*, 125:081104, 2006.

[21] A. J. Cohen, P. Mori-Sánchez, and W. Yang. *Science*, 321:792, 2008.

[22] P. Mori-Sánchez, Q. Wu, and W. Yang. *J. Chem. Phys.*, 119:11001, 2003.

[23] Y. Zhang and W. Yang. *J. Chem. Phys.*, 109:2604, 1998.

[24] A. J. Cohen, P. Mori-Sánchez, and W. Yang. *J. Chem. Phys.*, 126:191109, 2007.

[25] A. J. Cohen, P. Mori-Sánchez, and W. Yang. *Phys. Rev. B*, 77:115123, 2008.

[26] P. Mori-Sánchez, A. J. Cohen, and W. Yang. *Phys. Rev. lett.*, 100:146401, 2008.

[27] P. Mori-Sánchez, Q. Wu, and W. Yang. *J. Chem. Phys.*, 123:062204, 2005.

[28] D. C. Langreth and J. P. Perdew. *Phys. Rev. B*, 15:2884, 1977.

[29] W. Kohn, Y. Meir, and D. E. Makarov. *Phys. Rev. Lett.*, 80:4153, 1998.

[30] U. Von Barth and L. Hedin. *J. Phys. C*, 5:1629, 1972.

[31] M. M. Pant and A. K. Rajagopal. *Solid State Commun.*, 10:1157, 1972.

[32] A. K. Rajagopal and J. Callaway. *Phys. Rev. B*, 7:1912, 1973.

[33] P. W. Ayers and W. Yang. *J. Chem. Phys.*, 124:224108, 2006.

[34] T. Oda and A. Pasquarello. *Phys. Rev. Lett.*, 89:197204, 2002.

[35] R. C. Longo, E. G. Noya, and L. J. Gallego. *Phys. Rev. B*, 72:174409, 2005.

[36] Ph. Kurz, F. Förster, L. Nordström, G. Bihlmayer, and S. Blügel. *Phys. Rev. B*, 69:024415, 2004.

[37] S. Di Napoli, A. M. Llois, G. Bihlmayer, S. Blügel, M. Alouani, and H. Dreyssè. *Phys. Rev. B*, 70:174418, 2004.

[38] K. Nakamura, Y. Kato, T. Akiyama, and T. Ito. *Phys. Rev. Lett.*, 96:047206, 2006.

[39] K. Capelle and G. Vignale. *Phys. Rev. Lett.*, 86:5546, 2001.

[40] H. Eschrig and W. E. Pickett. *Solid State Commun.*, 118:123, 2001.

[41] K. Capelle and G. Vignale. *Phys. Rev. B*, 65:113106, 2002.

[42] W. Kohn, A. Savin, and C. A. Ullrich. *Int. J. Quantum Chem.*, 100:20, 2004.

[43] C. A. Ullrich. *Phys. Rev. B*, 72:073102, 2005.

[44] R. G. Parr and W. Yang. *Density-Functional Theory of Atoms and Molecules*. Oxford University Press, Oxford, 1989.

[45] G. Vignale and M. Rasolt. *Phys. Rev. B*, 37:10685, 1988.

[46] S. Erhard and E. K. U. Gross. *Phys. Rev. A*, 53:R5, 1996.

[47] G. Vignale and M. Rasolt. *Phys. Rev. Lett.*, 59:2360, 1987.

[48] W. Yang and Q. Wu. *Phys. Rev. Lett.*, 89:143002, 2002.

[49] S. Sharma, J. K. Dewhurst, C. Ambrosch-Draxl, N. Helbig, S. Kurth, E. K. U. Gross, S. Shallcross, and L. Nordströem. *cond-mat/0510800*, 2005.

[50] S. Rohra and A. Görling. *Phys. Rev. Lett.*, 97:013005, 2006.

[51] R. S. Mulliken. *J. Chem. Phys.*, 3:573, 1935.

[52] R. F. Stewart, E. R. Davidson, and W. Simpson. *J. Chem. Phys.*, 42:3175, 1965.

[53] F. L. Hirshfeld. *Theor. Chim. Acta*, 44:129, 1977.

[54] R. F. W. Bader and T. T. Nguyen-Dang. *Adv. Quantum Chem.*, 14:63, 1981.

[55] W. Yang and W. Mortier. *J. Am. Chem. Soc.*, 108:5708, 1986.

[56] P. Bultinck, S. Fias, C. Van Alsenoy, P. W. Ayers, and R. Carbó-Dorca. *J. Chem. Phys.*, 127:034102, 2007.

[57] R. G. Parr and W. Yang. *J. Am. Chem. Soc.*, 106:4049, 1984.

[58] S. M. Werden and E. R. Davidson. On the calculation of potentials from densities. In J. P. Dahl and J. Avery, editors, *Local Density Approximations in Quantum Chemistry*, pages 33–42. Plenum, 1984.

[59] Y. Wang and R. G. Parr. *Phys. Rev. A*, 47:R1591, 1992.

[60] R. van Leeuwen and E. J. Baerends. *Phys. Rev. A*, 49:2421, 1994.

[61] Q. Zhao, R. C. Morrison, and R. G. Parr. *Phys. Rev. A*, 50:2138, 1994.

[62] Q. Wu and W. Yang. *J. Chem. Phys.*, 118:2498, 2003.

[63] M. Wang, X. Hu, D. N. Beratan, and W. Yang. *J. Am. Chem. Soc.*, 128:3228, 2006.

[64] S. Keinan, X. Hu, D. N. Beratan, and W. Yang. *J. Phys. Chem. A*, 111:176, 2007.

[65] A. Tikhonov and V. Arsenin. *Solution of Ill-posed Problems*. Wiley, New York, 1977.

[66] C. W. Groetsch. *Inverse Problems in the Mathematical Sciences*. Vieweg-Verlag, Braunschweig, 1993.

[67] V. N. Staroverov, G. E. Scuseria, and E. R. Davidson. *J. Chem. Phys.*, 124:141103, 2006.

[68] A. F. Izmaylov, V. N. Staroverov, G. E. Scuseria, E. R. Davidson, G. Stoltz, and E. Cancès. *J. Chem. Phys.*, 126:084107, 2007.

[69] A. Heßelmann, A. W. Götz, F. Della Sala, and A. Görling. *J. Chem. Phys.*, 127:054102, 2007.

[70] A. Görling, A. Heßelmann, M. Jones, and M. Levy. *J. Chem. Phys.*, 128:104104, 2008.

[71] C. Kollmara and M. Filatov. *J. Chem. Phys.*, 127:114104, 2007.

[72] E. Cancès, G. Stoltz, G. E. Scuseria, V. N. Staroverov, and E. R. Davidson. *MathS In Action*, 2:1, 2009.

[73] S. Ivanov, S. Hirata, and R. J. Bartlett. *Phys. Rev. Lett.*, 83:5455, 1999.

[74] A. Görling. *Phys. Rev. Lett.*, 83:5459, 1999.

[75] S. Kummel and L. Kronik. *Phys. Mod. Phys.*, 80:3, 2008.

[76] S. Hirata, S. Ivanov, I. Grabowski, R. J. Bartlett, K. Burke, and J. D. Talman. *J. Chem. Phys.*, 115:1635, 2001.

[77] S. Ivanov and M. Levy. *J. Chem. Phys.*, 119:7087, 2003.

[78] T. Heaton-Burgess, F. A. Bulat, and W. Yang. *Phys. Rev. Lett.*, 98:256401, 2007.

[79] S. Hamel, M. E. Casida, and D. R. Salahub. *J. Chem. Phys.*, 116:8276, 2002.

[80] Q. Wu and W. Yang. *J. Theo. Comp. Chem.*, 2:627, 2003.

[81] E. Fermi and E. Amaldi. *Acad. Ital. Rome*, 6:117, 1934.

[82] Q. Wu, P. W. Ayers, and W. Yang. *J. Chem. Phys.*, 119:2978, 2003.

[83] T. Heaton-Burgess, A. J. Cohen, W. Yang, and E. R. Davidson. *J. Chem. Phys.*, 128:114702, 2008.

[84] T. Heaton-Burgess, F. A. Bulat, and W. Yang. *Phys. Rev. Lett.*, 98:256401, 2007.

[85] P. C. Hansen. *Rank-Deficient and Discrete Ill-Posed Problems.* SIAM, PA, 1989.

[86] F. A. Bulat, T. Heaton-Burgess, A. J. Cohen, and W. Yang. *J. Chem. Phys.*, 127:174101, 2007.

[87] P. Mori-Sánchez, Q. Wu, and W. Yang. *J. Chem. Phys.*, 119:11001, 2003.

[88] Q. Wu, A. J. Cohen, and W. Yang. *Mol. Phys.*, 103:711, 2005.

[89] P. C. Hansen and D. P. O'Leary. *SIAM J. Sci. Comput.*, 14:1487, 1993.

[90] High Performance Computational Chemistry Group. NWChem, *A Computational Chemistry Package for Parallel Computers*, version 4.6; Pacific Northwest National Laboratory: Richland, WA 99352, 2004.

[91] J. C. Slater. *Quantum Theory of Molecules and Solids*. McGraw-Hill, New York, 1974.

[92] T. H. Dunning, Jr. *J. Chem. Phys.*, 90:1007, 1989.

[93] H. Partridge. *J. Chem. Phys.*, 87:6643, 1987.

[94] S. Ivanov, S. Hirata, and R. J. Bartlett. *J. Chem. Phys.*, 116:1269, 2002.

[95] C. Kollmara and M. Filatov. *J. Chem. Phys.*, 127:114104, 2007.

[96] S. K. Ghosh and R. G. Parr. *J. Chem. Phys.*, 82:3307, 1985.

[97] M. Levy and J. P. Perdew. *Phys. Rev. A*, 32:2010, 1985.

[98] NIST Computational Chemistry Comparison and Benchmark Database, NIST Standard Reference Database Number 101, Release 12, Aug 2005, Editor: Russell D. Johnson III, http://srdata.nist.gov/cccbdb.

[99] M. E. Casida, C. Jamorski, K. C. Casida, and D. R. Salahub. *J. Chem. Phys.*, 108:4439, 1998.

[100] R. Ahlrichs, M. Hoffmann-Ostenhof, T. Hoffmann-Ostenhof, and J. D. Morgan. *Phys. Rev. A*, 23:2106, 1981.

[101] C. O. Almbladh and U. von Barth. *Phys. Rev. B*, 31:3231, 1985.

[102] J. Katriel and E. R. Davidson. *Proc. Natl. Acad. Sci. U.S.A.*, 77:4403, 1980.

[103] M. M. Morrell, R. G. Parr, and M. Levy. *J. Chem. Phys.*, 62:549, 1975.

[104] Q. Wu, P. W. Ayers, and W. Yang. *J. Chem. Phys.*, 119:2978, 2003.

[105] F. Della Salaa and A. Görling. *J. Chem. Phys.*, 116:5374, 2002.

[106] D. R. Rohr, O. V. Gritsenko, and E. Jan Baerends. *J. Mol. Struct. (THEOCHEM)*, 762:193, 2006.

[107] A. D. Becke. *Phys. Rev. A*, 38:3098, 1988.

[108] S. Kümmel and J. P. Perdew. *Phys. Rev. Lett.*, 90:043004, 2003.

[109] D. E. Woon and T. H. Dunning, Jr. *J. Chem. Phys.*, 98:1358, 1993.

[110] T. Heaton-Burgess, F. A. Bulat, and W. Yang. *Phys. Rev. Lett.*, 98:256401, 2007.

[111] D. Jacquemin, A. Femenias, H. Chermette, I. Ciofini, C. Adamo, J.-M. Andr, and E. A. Perpète. *J. Phys. Chem. A*, 110:5952, 2006.

[112] D. Jacquemin, E. A. Perpte, G. Scalmani, M. J. Frisch, and R. Kobayashi. *J. Chem. Phys.*, 126:144105, 2007.

[113] T. Torelli and L. Mitas. *Phys. Rev. Lett.*, 85:1702, 2000.

[114] J. Hutter, H. P. Luethi, and F. Diederich. *J. Am. Chem. Soc.*, 116:750, 1994.

[115] J. M. L. Martin, J. El-Yazal, and J. P. Franois. *Chem. Phys. Lett.*, 242:570, 1995.

[116] M. Saito and Y. Okamoto. *Phys. Rev. B*, 60:8939, 1999.

[117] S. Sen, P. Seal, and S. Chakrabarti. *Phys. Rev. B.*, 73:245401, 2006.

[118] S. Arulmozhirajaa and T. Ohno. *J. Chem. Phys.*, 128:114301, 2008.

[119] K. Raghavachari, D. L. Strout, G. K. Odom, G. E. Scuseria, J. A. Pople, B. G. Johnson, and P. M. W. Gill. *Chem. Phys. Lett.*, 214:357, 1993.

[120] J. C. Grossman, L. Mitas, and K. Raghavachari. *Phys. Rev. Lett.*, 75:3870, 1995.

[121] Z. Wang, P. Day, and R. Pachter. *Chem. Phys. Lett.*, 248:121, 1996.

[122] P. Mori-Sánchez, Q. Wu, and W. Yang. *J. Chem. Phys.*, 119:11001, 2003.

[123] E. R. Johnson, P. Mori-Sánchez, A. J. Cohen, and W. Yang. *J. Chem. Phys.*, 129:204112, 2008.

[124] J. P. Perdew, R. G. Parr, M. Levy, and J. L. Balduz, Jr. *Phys. Rev. Lett.*, 49:1691, 1982.

[125] W. Yang, Y. Zhang, and P. W. Ayers. *Phys. Rev. Lett.*, 84:5172, 2000.

[126] D. Jacquemina, E. A. Perpète, H. Chermetteb, I. Ciofinic, and C. Adamo. *Chem. Phys.*, 332:79, 2007.

[127] E. J. Bylaska, J. H. Weare, and R. Kawai. *Phys. Rev. B*, 58:R7488, 1998.

[128] T. Yanai, D. P. Tew, and N. C. Handy. *Chem. Phys. Lett.*, 393:51, 2004.

[129] DALTON, a molecular electronic structure program, Release 2.0 (2005), see http://www.kjemi.uio.no/software/dalton/dalton.html.

[130] W. An, Y. Gao, S. Bulusu, and X. C. Zeng. *J. Chem. Phys.*, 122:204109, 2005.

Biography

Personal

Full name: Timothy James Heaton-Burgess
Born: 18 March 1981 in Blenheim, New Zealand

Education

Ph.D. (2009)
in Chemistry, Duke University

B.Sc. (Hons.) (2003)
in Chemistry and Mathematical Physics, University of Canterbury

Publications

- Tim Heaton-Burgess, Paul W. Ayers, and Weitao Yang, "Spin-Potential Functional Formalism for Current-Carrying Noncollinear Magnetic Systems", *Phys. Rev. Lett.*, **98**, 036403 (2007)
- Tim Heaton-Burgess, Felipe A. Bulat, and Weitao Yang, "Optimized Effective Potentials in Finite Basis Sets", *Phys. Rev. Lett.*, **98**, 256401 (2007)
- Felipe A. Bulat, Tim Heaton-Burgess, Aron J. Cohen and Weitao Yang, "Optimized Effective Potentials from Electron Densities in Finite Basis Sets,", *J. Chem. Phys.* **127**, 174101 (2007)

- Tim Heaton-Burgess, Aron J. Cohen, Weitao Yang, and Ernest R. Davidson, "Size Extensivity of the Direct Optimized Effective Potential Method" *J. Chem. Phys.*, **128**, 114702 (2008)
- Tim Heaton-Burgess and Weitao Yang, "Optimized Effective Potentials from Arbitrary Basis Sets", *J. Chem. Phys.*, **129**, 194102 (2008)
- Tim Heaton-Burgess and Weitao Yang, "A Manifestation of the Delocalization Error of Density Functional Approximations: Structures of C_{4N+2} Rings", in preparation.

Awards

2007	Kathleen Zielek Fellowship
2004–2006	Lord Rutherford Memorial Research Fellowship